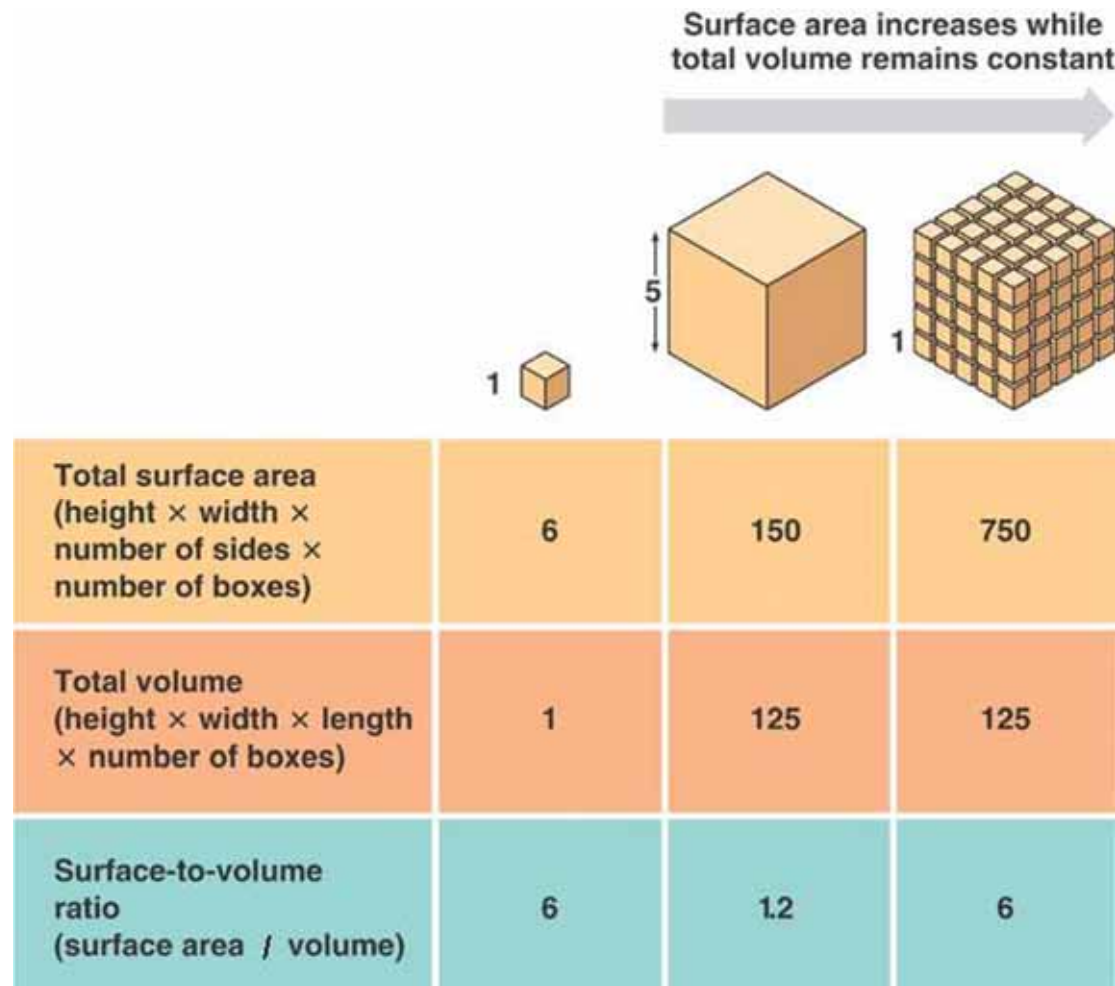


Nanomaterials

- Metals and Alloys
 - Fe, Al, Au
- Semiconductors
 - Band gap, CdS, TiO₂, ZnO
- Ceramic
 - Al₂O₃, Si₃N₄, MgO, , SiO₂, ZrO₂
- Carbon based
 - Diamond, graphite, nanotube, C60, graphene
- Polymers
 - Soft mater, block co-polymer
- Biological
 - Photonic, hydrophobic, adhesive,
- Composites

Surface to Volume Ratio



Surface Energy

One face surface energy: γ

27 cube: $27 \times 6 \gamma$

3 x 9 cube line: 114γ

3 x (3x3) square: 90γ

3 x 3 x 3 cube: 54γ

Surface to Volume Ratio

Au: AAA

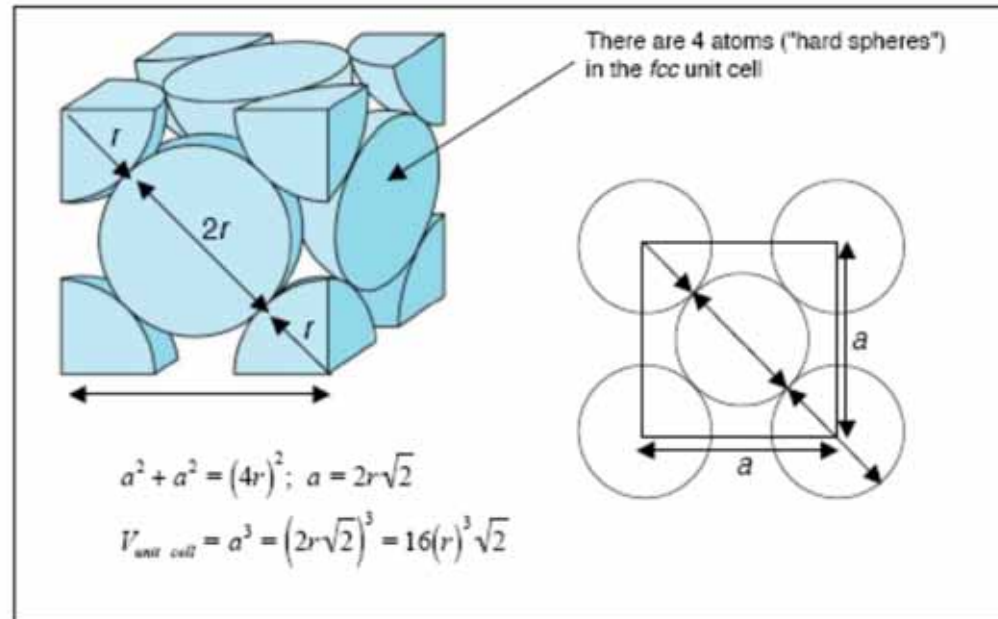
Atomic mass: 196.967

Density 19.31

Radii =0.144 nm

Number of Au atoms in 1 m	$3.4 \cdot 10^9$
Volume of Au atom	$4.19 \cdot 10^{28}$
Surface area Au atom	$7.22 \cdot 10^{19}$
Surface/volume ratio	$1.72 \cdot 10^{-9}$

fcc



$$V_{\text{unit cell}} = a^3 = (2r\sqrt{2})^3 = 16(0.5\text{nm})^3 \sqrt{2} = 2.828 \text{ nm}^3$$

$$\frac{10^{27} \text{ nm}^3}{2.828 \text{ nm}^3} = 3.536 \times 10^{26} \text{ nano unit cells}$$

$$\frac{S_{\text{spheres}}}{S_{\text{unit cell}}} = \frac{4.44 \times 10^9 \text{ m}^2}{6.0 \times 10^9 \text{ m}^2} = 0.74$$

$$\text{Collective Area} = 3.536 \times 10^{26} \text{ nano unit cells} \left(\frac{4 \text{ spheres}}{\text{unit cell}} \right) \left(\frac{4\pi r^2}{\text{sphere}} \right) = 4.44 \times 10^{27} \text{ nm}^2$$

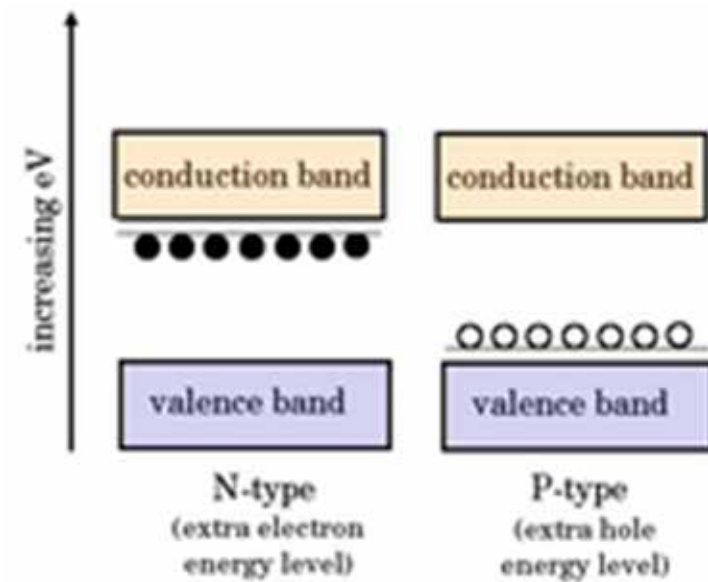
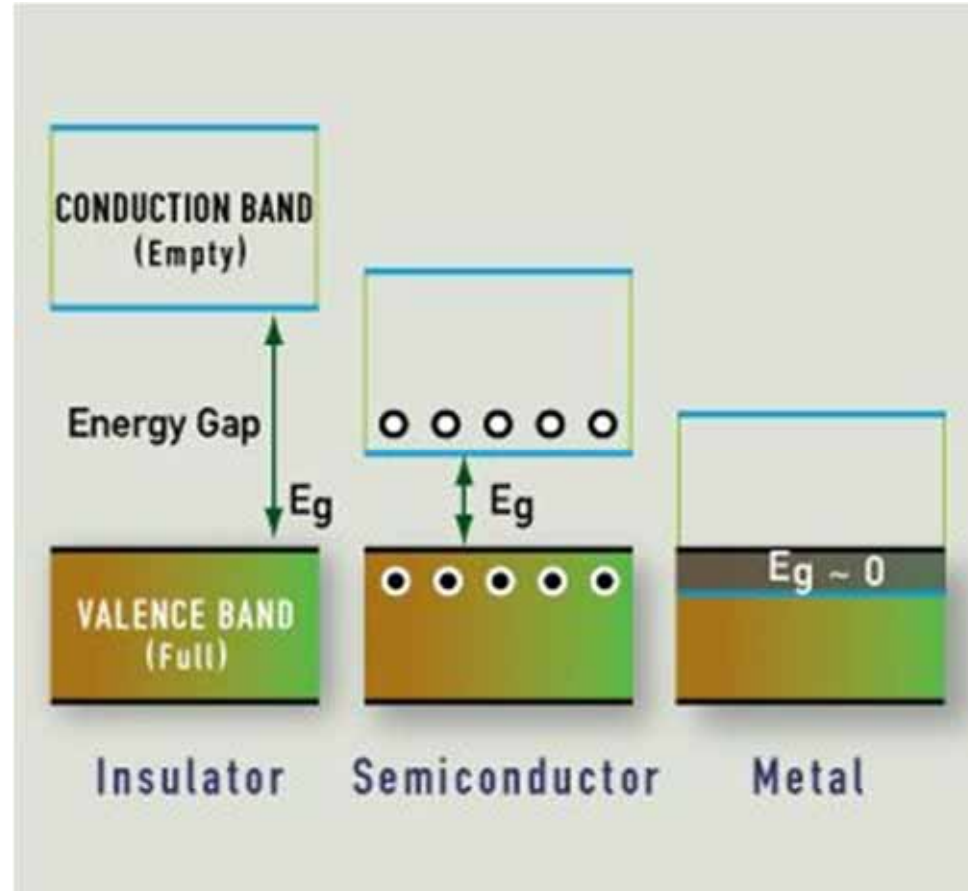
Packing Fraction

$$\text{APF} = \frac{N_{\text{atoms}} V_{\text{atom}}}{V_{\text{crystal}}}$$

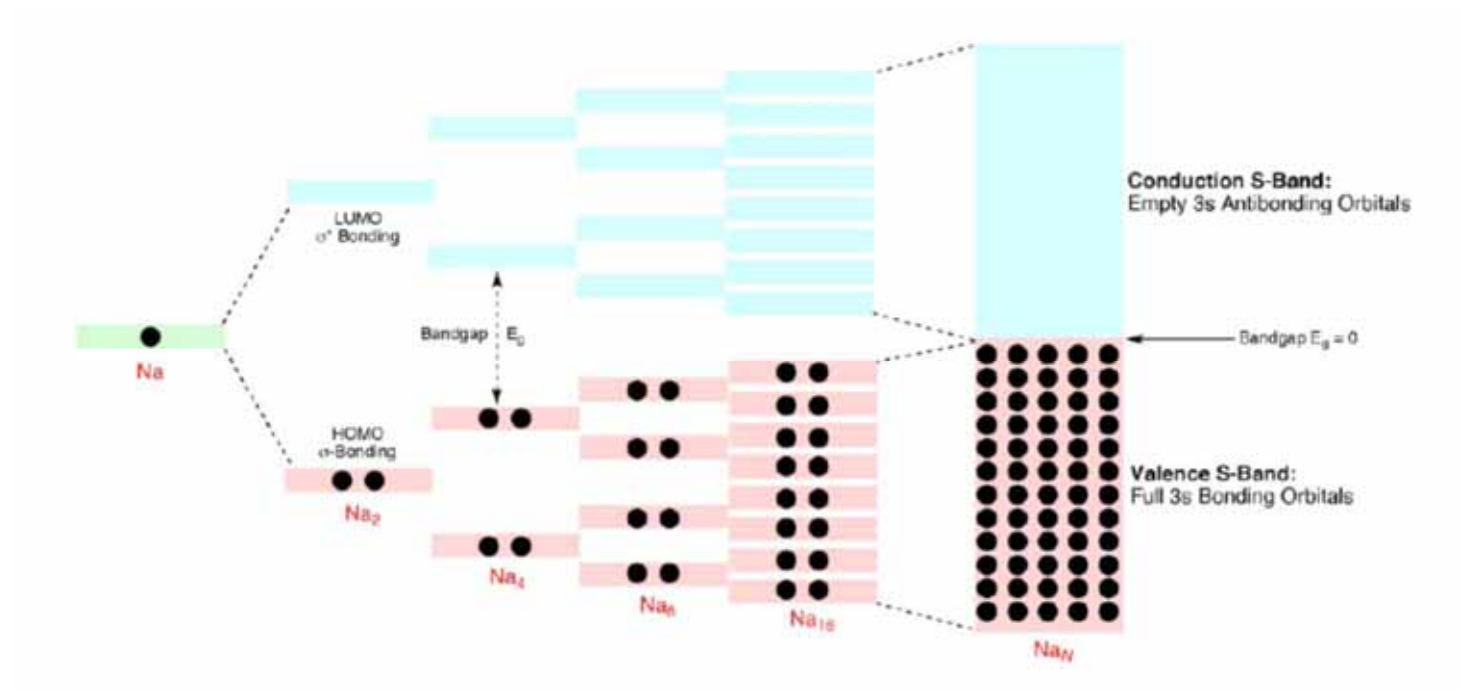
Surfaces

- Collective surface area of nanocube 1 nm
- Porous materials
 - Micropore (<2 nm)
 - Mesopore (2 nm ~ 50 nm)
 - Marcopore (> 50nm)
- Void volume
 - $V_{\text{pore}}/V_{\text{material}}$

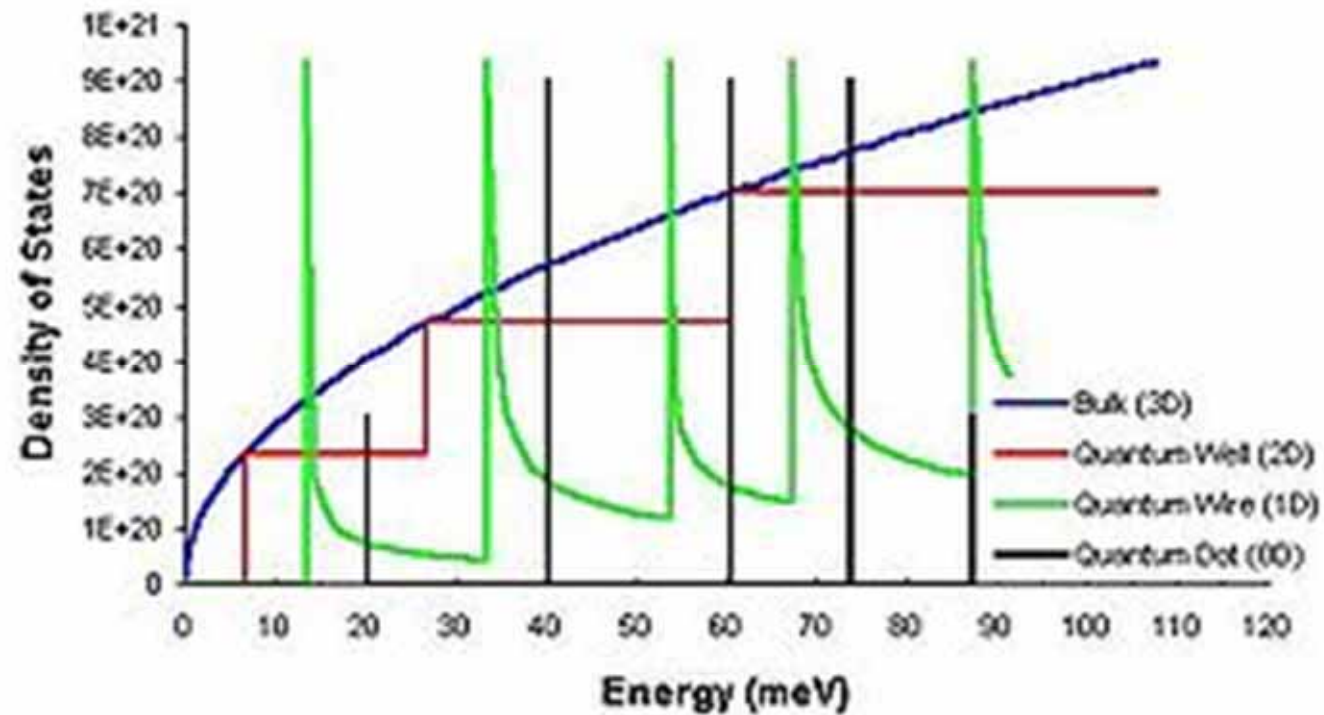
Bandgap



Bandgap



Density of State

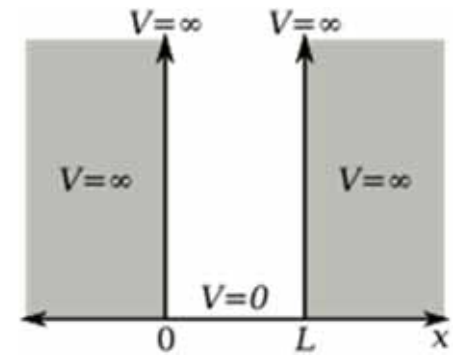


Particle in a Box

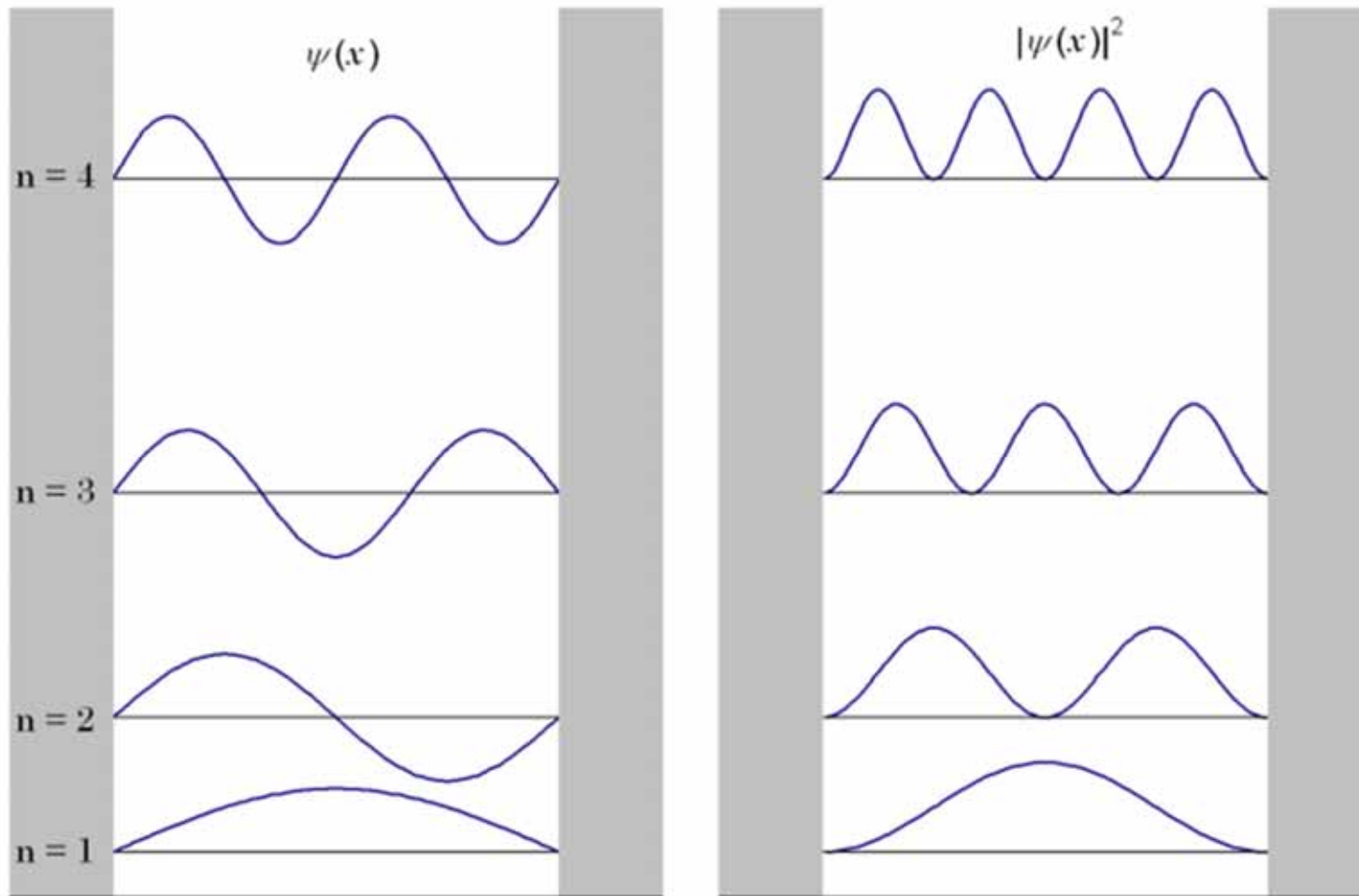
$$-\frac{\hbar^2}{2m} \frac{d^2\psi(x)}{dx^2} + V(x)\psi(x) = E\psi(x) \quad (1)$$

$$\psi_n = \sqrt{\frac{2}{L}} \sin\left(\frac{n\pi x}{L}\right)$$

$$E_n = \frac{\hbar^2 \pi^2}{2mL^2} n^2$$



Particle in a Box



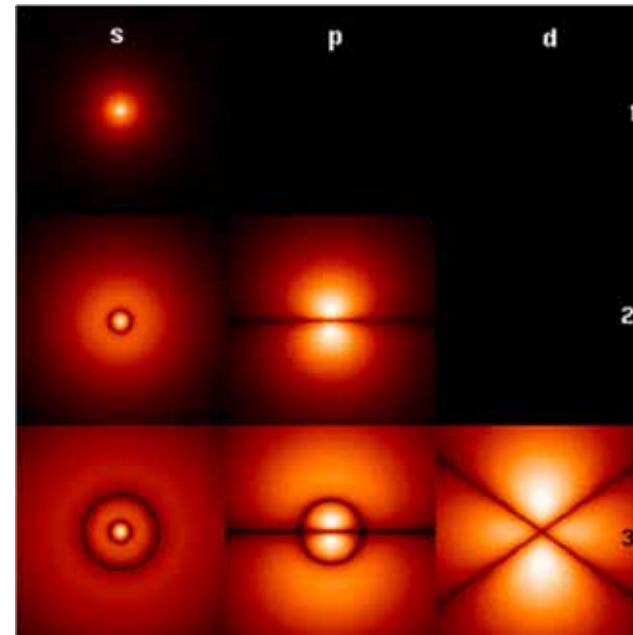
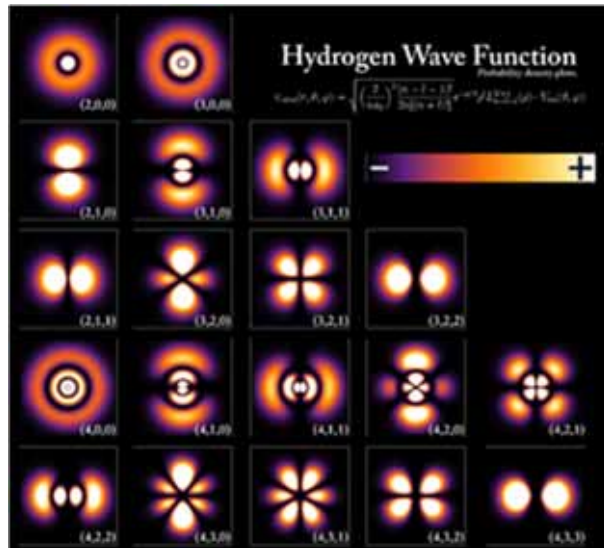
$$\psi_{n_x, n_y} = \sqrt{\frac{4}{L_x L_y}} \sin\left(\frac{n_x \pi x}{L_x}\right) \sin\left(\frac{n_y \pi y}{L_y}\right)$$

$$E_{n_x, n_y} = \frac{\hbar^2 \pi^2}{2m} \left[\left(\frac{n_x}{L_x}\right)^2 + \left(\frac{n_y}{L_y}\right)^2 \right]$$

$$\psi_{n_x, n_y, n_z} = \sqrt{\frac{8}{L_x L_y L_z}} \sin\left(\frac{n_x \pi x}{L_x}\right) \sin\left(\frac{n_y \pi y}{L_y}\right) \sin\left(\frac{n_z \pi z}{L_z}\right) \quad (22)$$

$$E_{n_x, n_y, n_z} = \frac{\hbar^2 \pi^2}{2m} \left[\left(\frac{n_x}{L_x}\right)^2 + \left(\frac{n_y}{L_y}\right)^2 + \left(\frac{n_z}{L_z}\right)^2 \right] \quad (23)$$

Wave Functions



$$i\hbar \frac{\partial}{\partial t} \Psi(\mathbf{r}, t) = \hat{H} \Psi = \left(-\frac{\hbar^2}{2m} \nabla^2 + V(\mathbf{r}) \right) \Psi(\mathbf{r}, t) = -\frac{\hbar^2}{2m} \nabla^2 \Psi(\mathbf{r}, t) + V(\mathbf{r}) \Psi(\mathbf{r}, t)$$

$$V(r) = -\frac{1}{4\pi\epsilon_0} \frac{Ze^2}{r}$$

$$\psi_{n\ell m}(r, \vartheta, \varphi) = \sqrt{\left(\frac{2}{na_0}\right)^3 \frac{(n-\ell-1)!}{2n(n+\ell)!}} e^{-\rho/2} \rho^\ell L_{n-\ell-1}^{2\ell+1}(\rho) \cdot Y_\ell^m(\vartheta, \varphi)$$

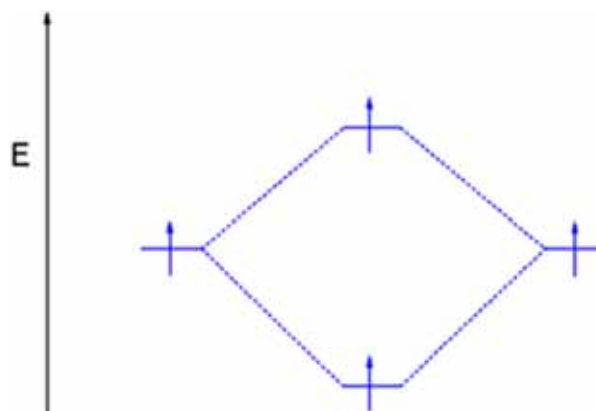
Linear combination of atomic orbitals molecular orbital method

$$\phi_i = c_{1i}\chi_1 + c_{2i}\chi_2 + c_{3i}\chi_3 + \cdots + c_{ni}\chi_n$$

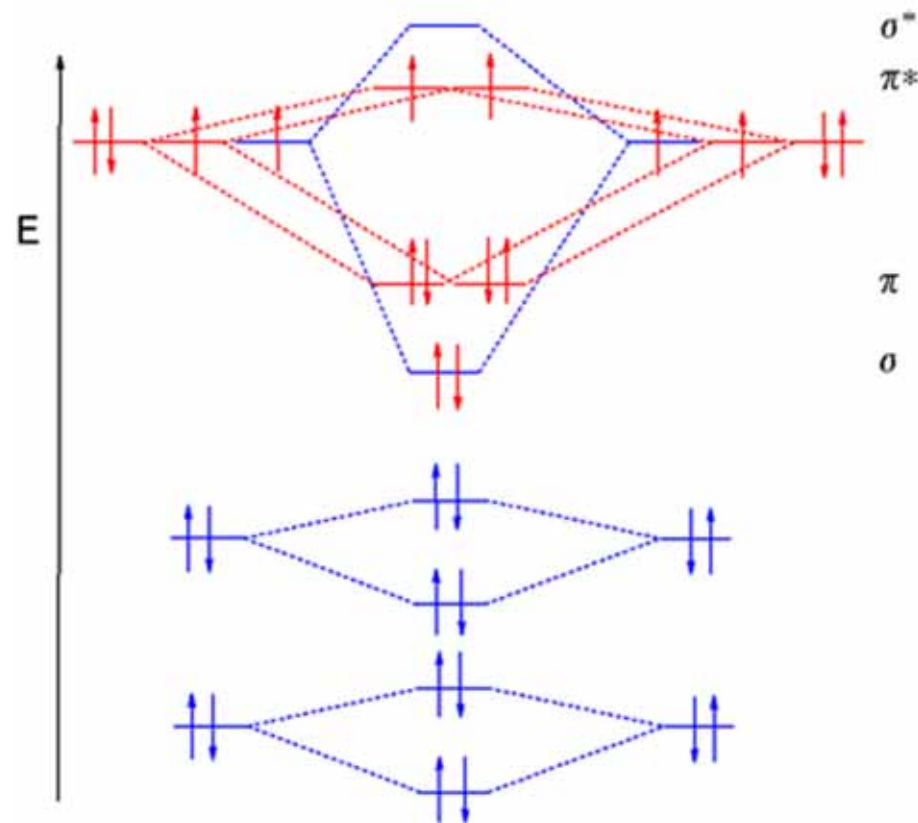
$$\psi_i = \sum_{\mu} c_{\mu i} \phi_{\mu}$$

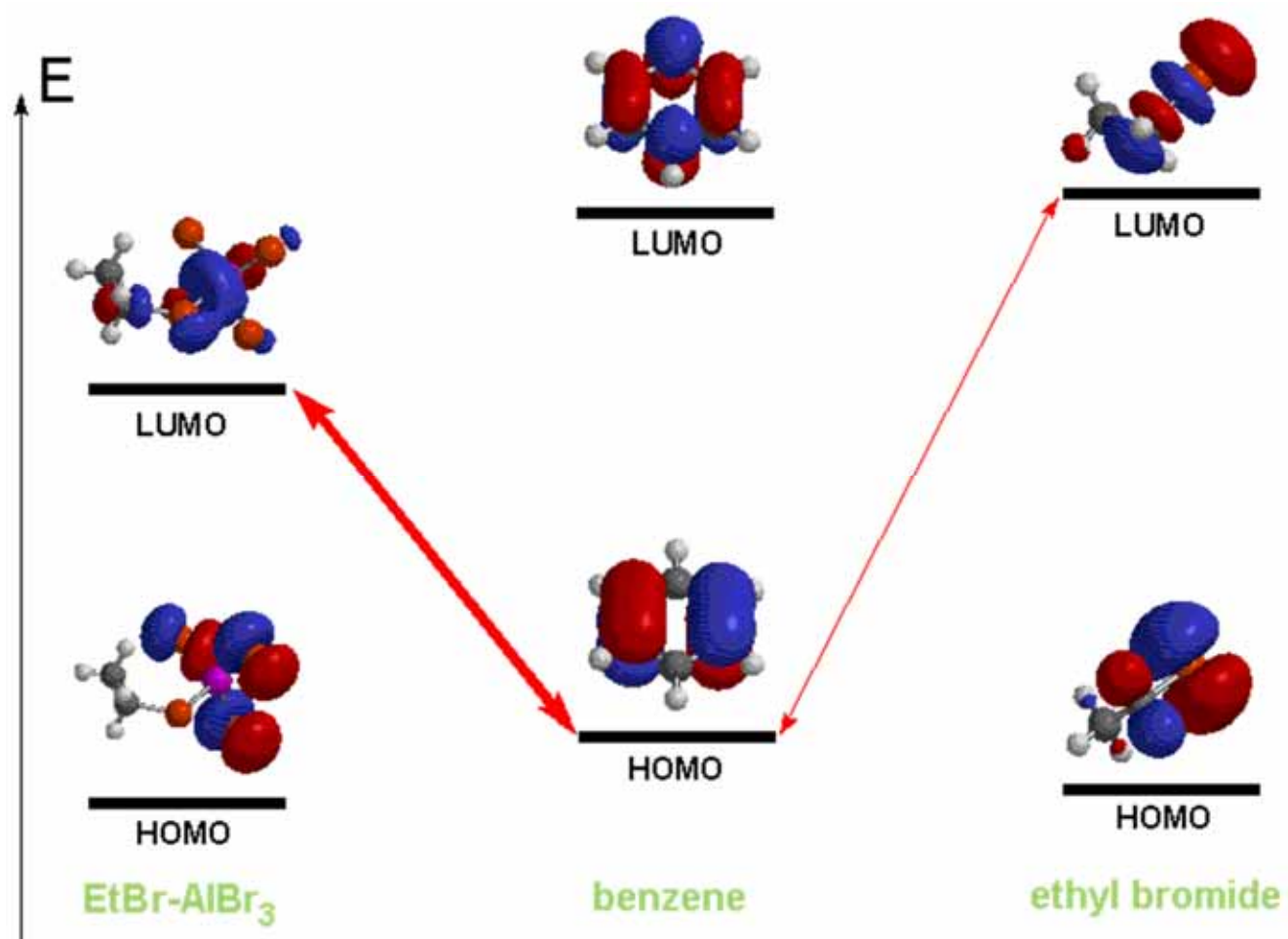
MO \nearrow ψ_i \nwarrow AO

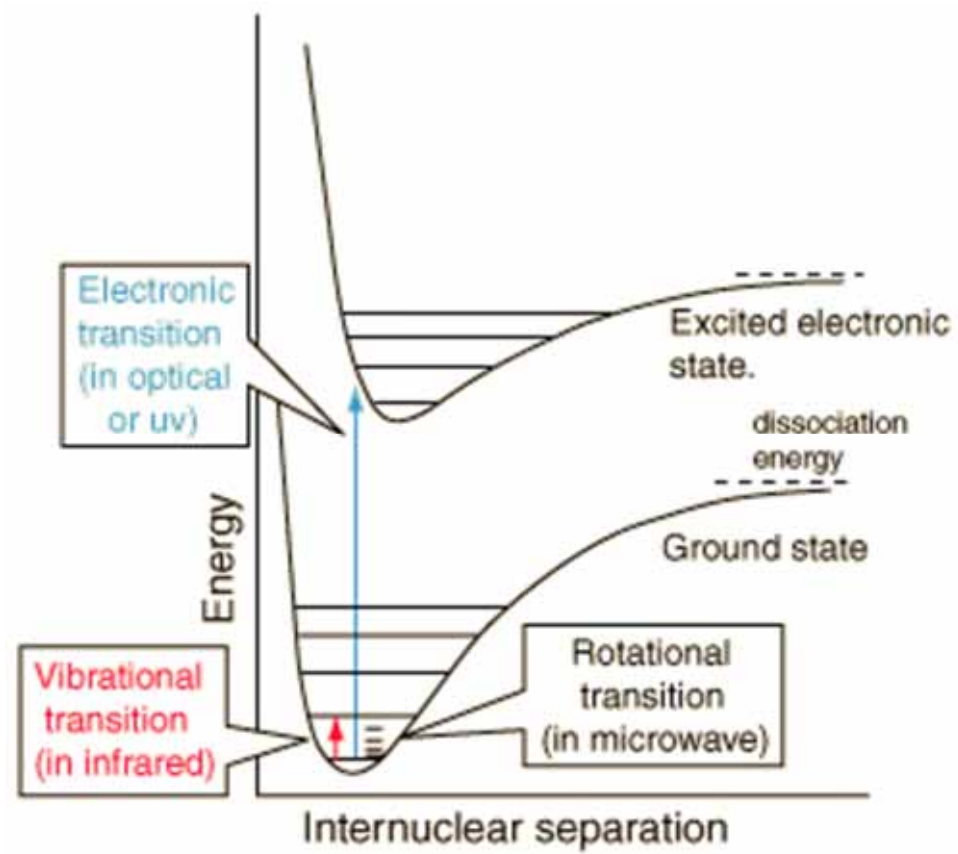
coefficient of AO_{μ} in MO_i \nearrow $c_{\mu i}$



Oxygen







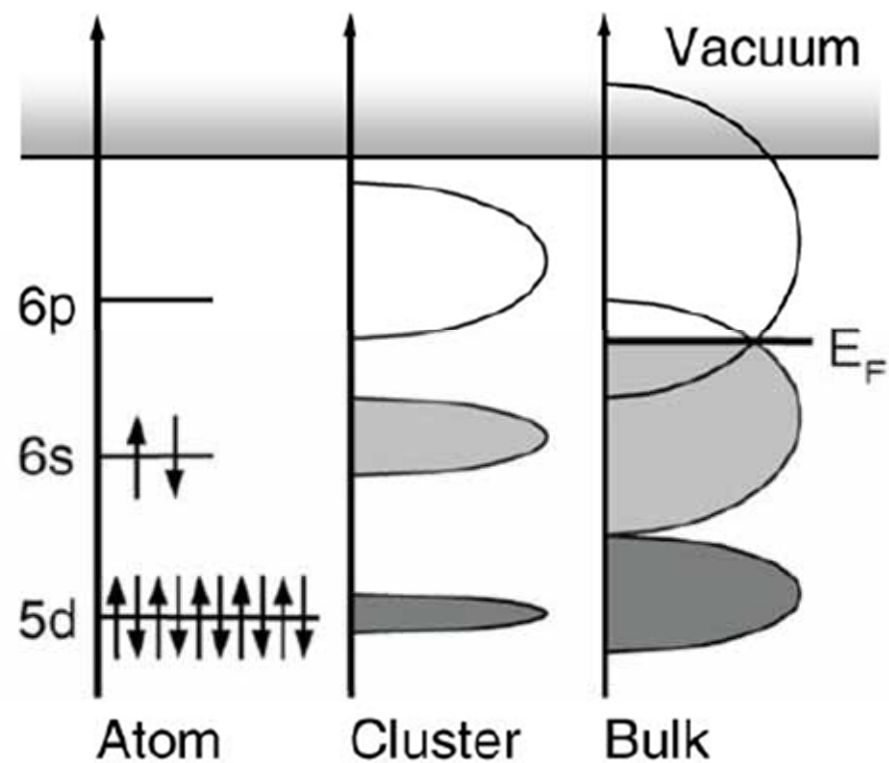


Figure 5 Energy diagram describing a generic Bloch-Wilson MIT in clusters (with specific reference to the energy levels of mercury). For sufficiently large clusters, the *s-p* band gap closes with increasing cluster size (shaded areas represent energy range with occupied electron levels). Overlap leads to a “continuous” DOS at E_F and to an Insulator to Metal transition.

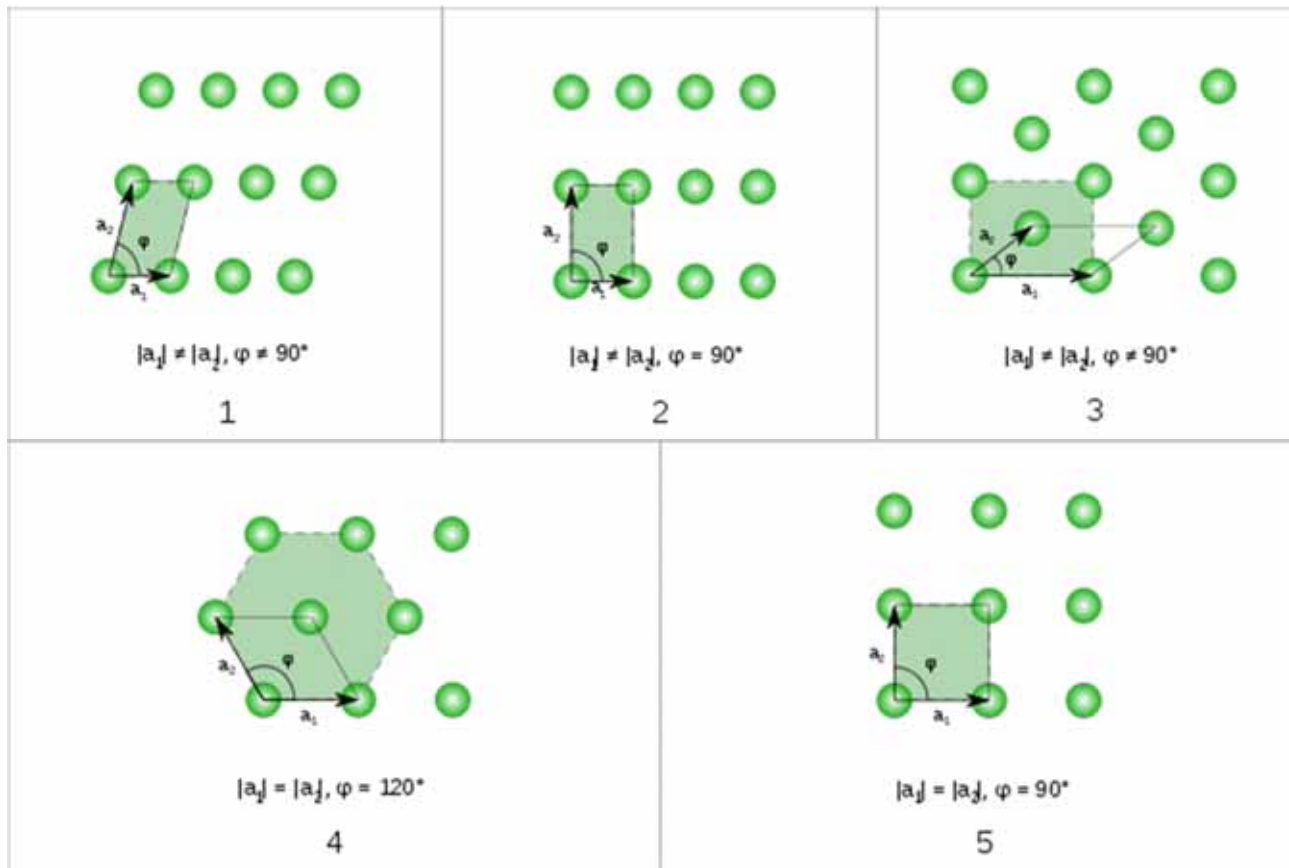
Bloch wave

$$\psi_{n\mathbf{k}}(\mathbf{r}) = e^{i\mathbf{k}\cdot\mathbf{r}} u_{n\mathbf{k}}(\mathbf{r})$$

A **Bloch wave** or **Bloch state**, named after [Felix Bloch](#), is the [wavefunction](#) of a particle (usually, an [electron](#)) placed in a [periodic potential](#).

$$\epsilon_n(\mathbf{k}) = \epsilon_n(\mathbf{k} + \mathbf{K}),$$

The five fundamental two-dimensional Bravais lattices



Unit Cell

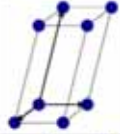
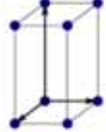

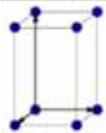
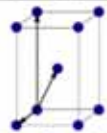
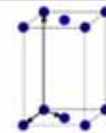
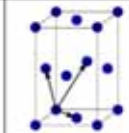
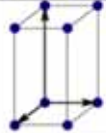
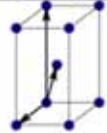

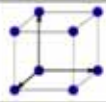
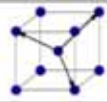

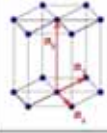
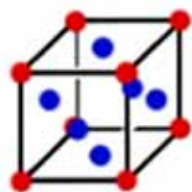
Bravais lattice	Parameters	Simple (P)	Volume centered (I)	Base centered (C)	Face centered (F)
Triclinic	$a_1 \neq a_2 \neq a_3$ $\alpha_{12} \neq \alpha_{23} \neq \alpha_{31}$				
Monoclinic	$a_1 \neq a_2 \neq a_3$ $\alpha_{23} = \alpha_{31} = 90^\circ$ $\alpha_{12} \neq 90^\circ$				
Orthorhombic	$a_1 \neq a_2 \neq a_3$ $\alpha_{12} = \alpha_{23} = \alpha_{31} = 90^\circ$				
Tetragonal	$a_1 = a_2 \neq a_3$ $\alpha_{12} = \alpha_{23} = \alpha_{31} = 90^\circ$				
Trigonal	$a_1 = a_2 = a_3$ $\alpha_{12} = \alpha_{23} = \alpha_{31} < 120^\circ$				
Cubic	$a_1 = a_2 = a_3$ $\alpha_{12} = \alpha_{23} = \alpha_{31} = 90^\circ$				
Hexagonal	$a_1 = a_2 \neq a_3$ $\alpha_{12} = 120^\circ$ $\alpha_{23} = \alpha_{31} = 90^\circ$				

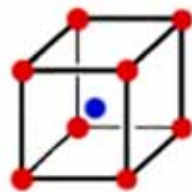
Table 1.1: Bravais lattices in three-dimensions.



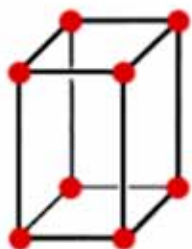
**Simple
cubic**



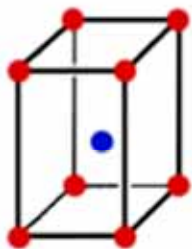
**Face-centered
cubic**



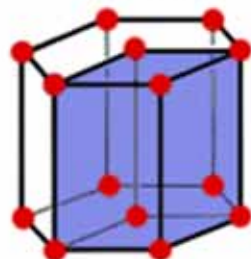
**Body-centered
cubic**



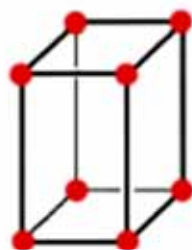
**Simple
tetragonal**



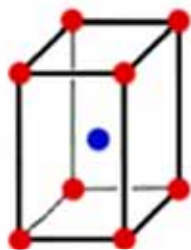
**Body-centered
tetragonal**



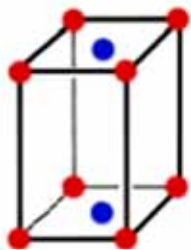
Hexagonal



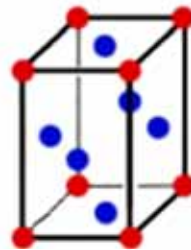
**Simple
orthorhombic**



**Body-centered
orthorhombic**



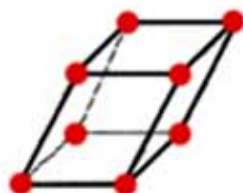
**Base-centered
orthorhombic**



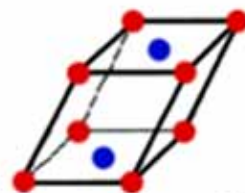
**Face-centered
orthorhombic**



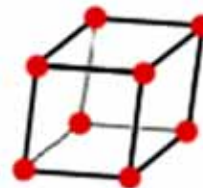
Rhombohedral



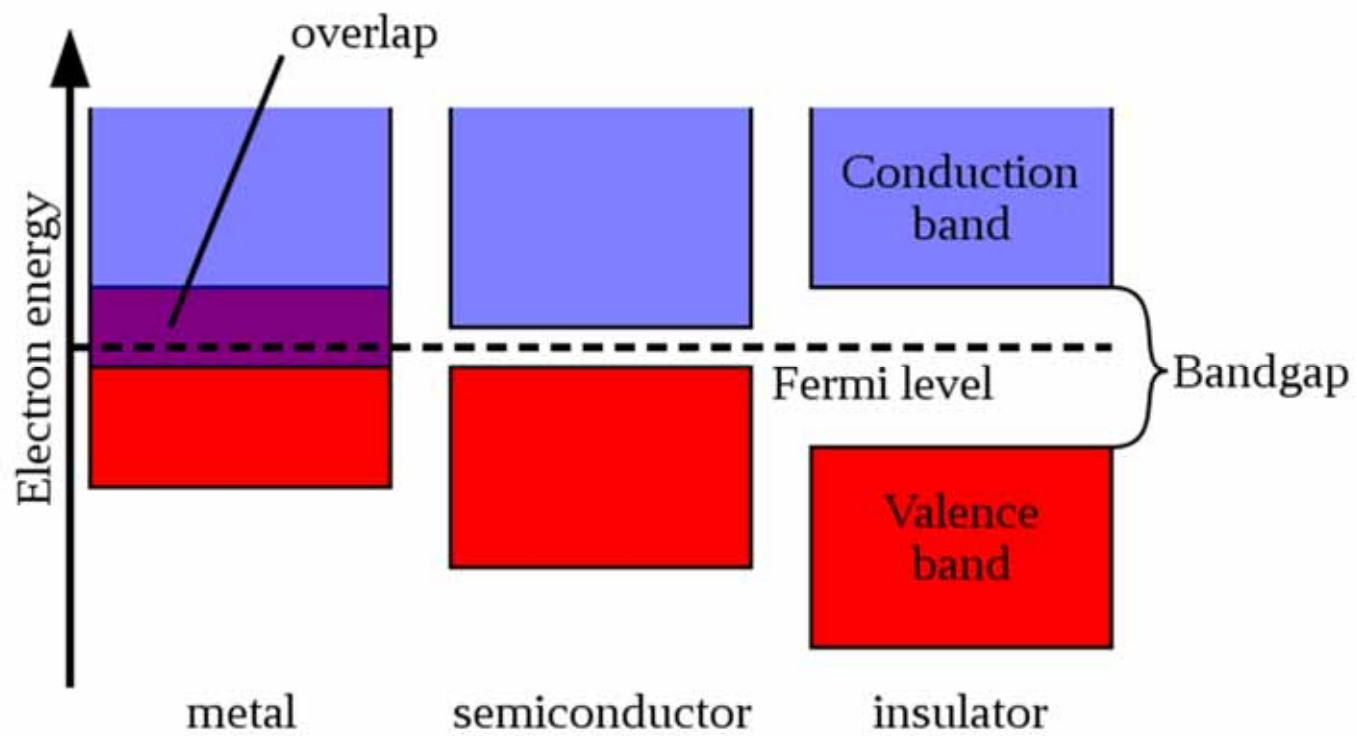
**Simple
Monoclinic**



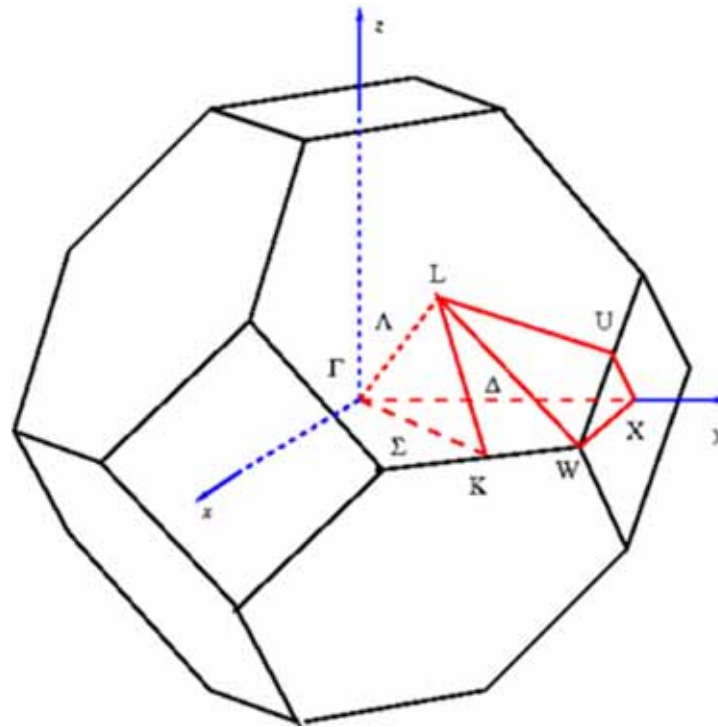
**Base-centered
monoclinic**



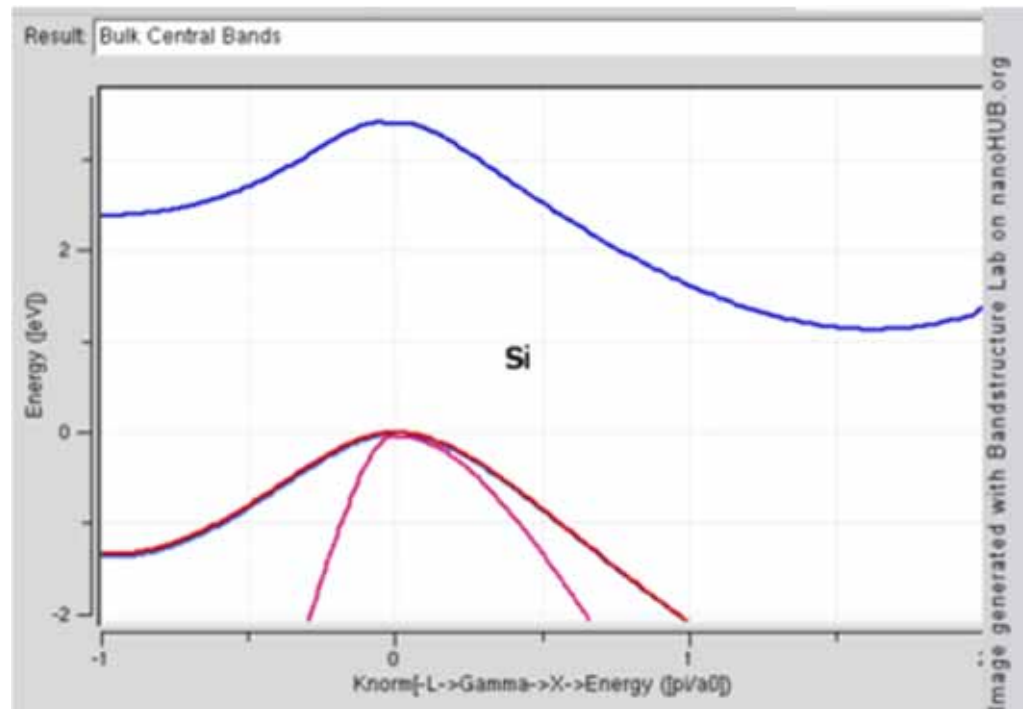
Triclinic



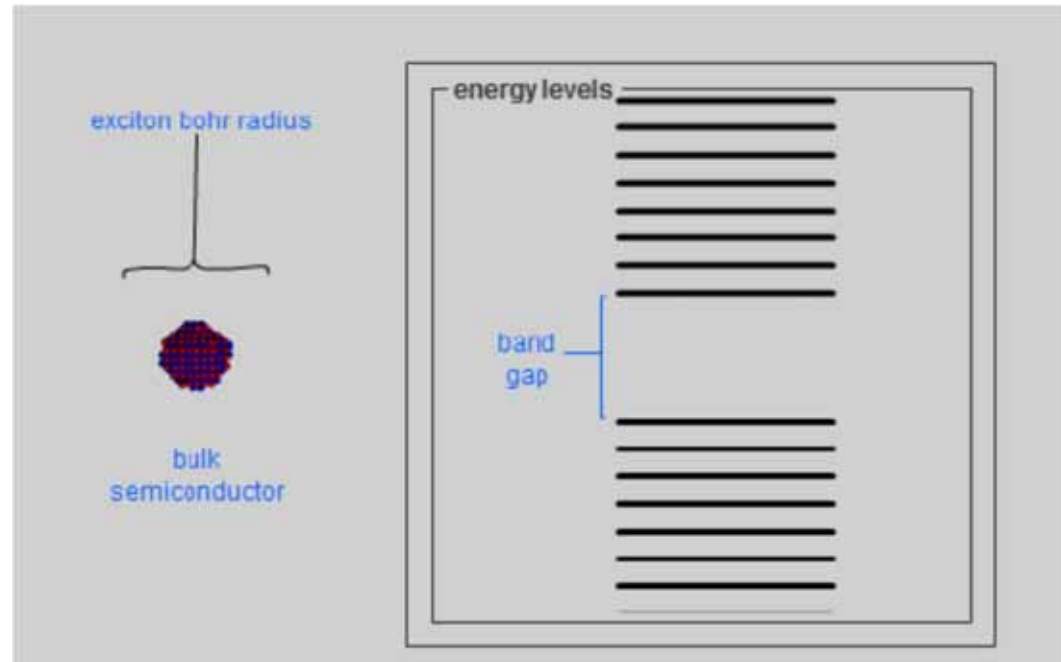
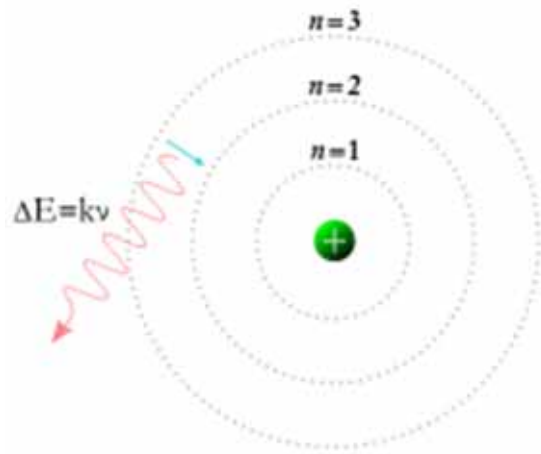
First Brillouin zone of FCC lattice showing symmetry labels



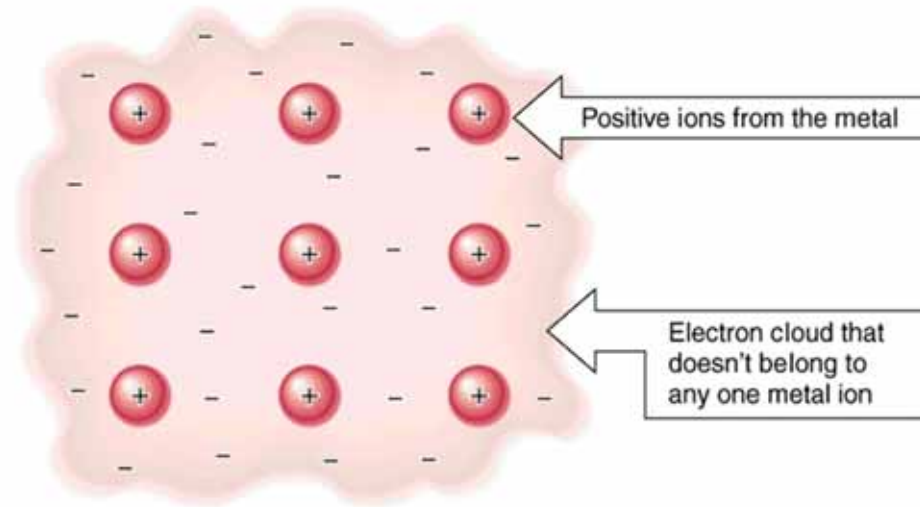
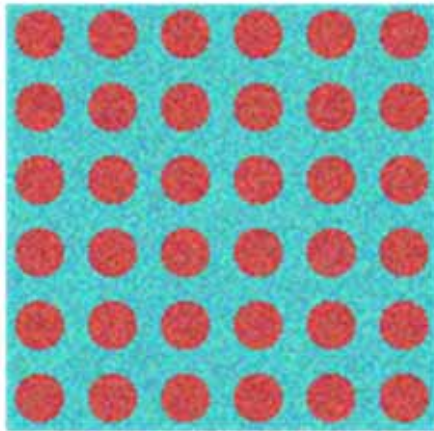
Band Structures



Bohr Exciton Radius



Electron Sea

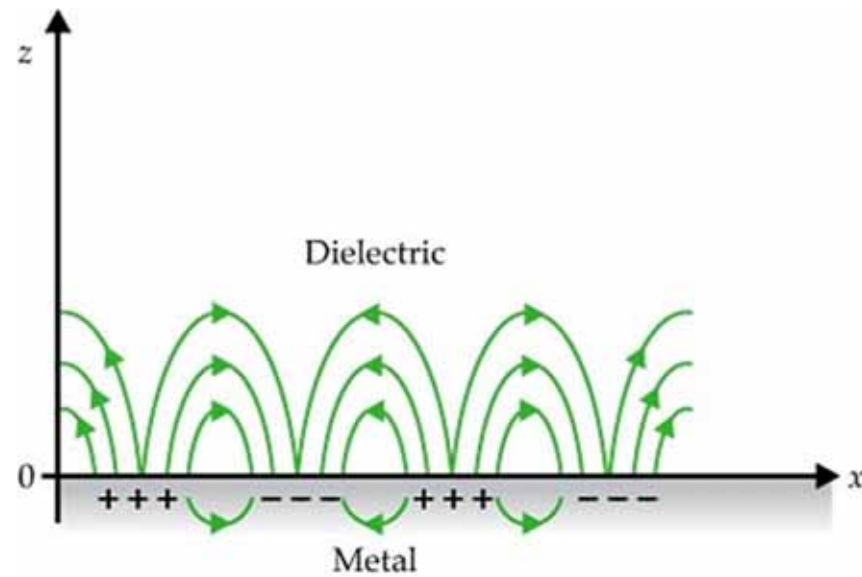


Copyright 1998 by John Wiley and Sons, Inc. All rights reserved.

$$m \frac{d^2 \delta x}{dt^2} = e E_x = -m \omega_p^2 \delta x,$$

$$\omega_p^2 = \frac{n e^2}{\epsilon_0 m},$$

Surface Plasmon



$$\epsilon_m = 1 - \frac{\omega_p^2}{\omega^2}$$

TiO₂

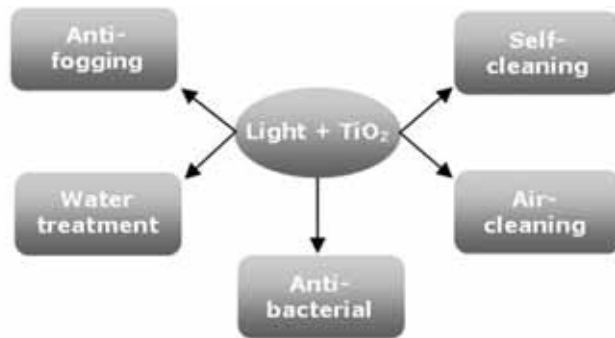
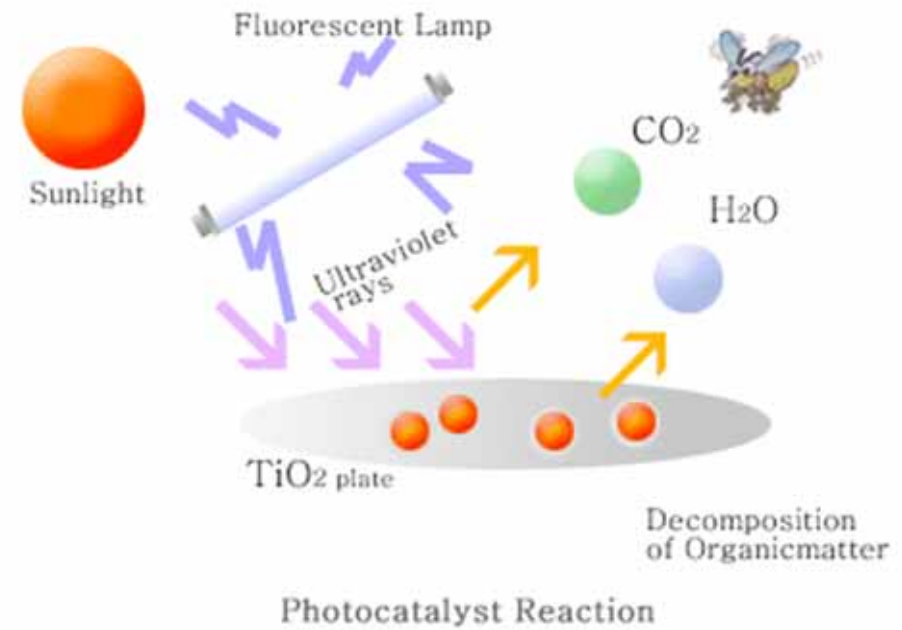
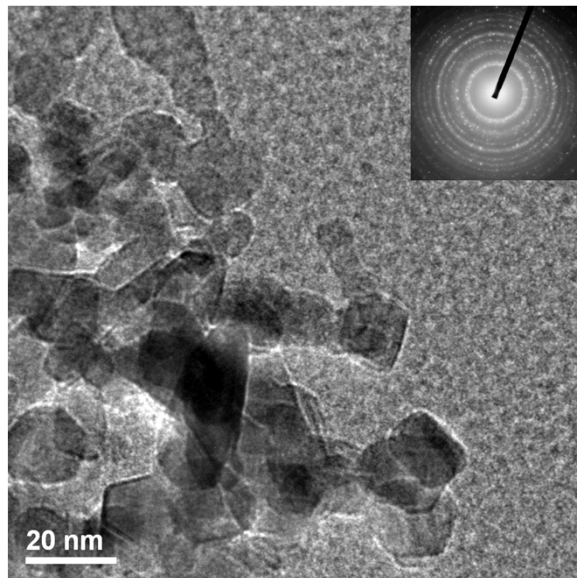


Figure 1. Major areas of activity in titanium dioxide photocatalysis



Carbon



SWNT



Poly-C₆₀

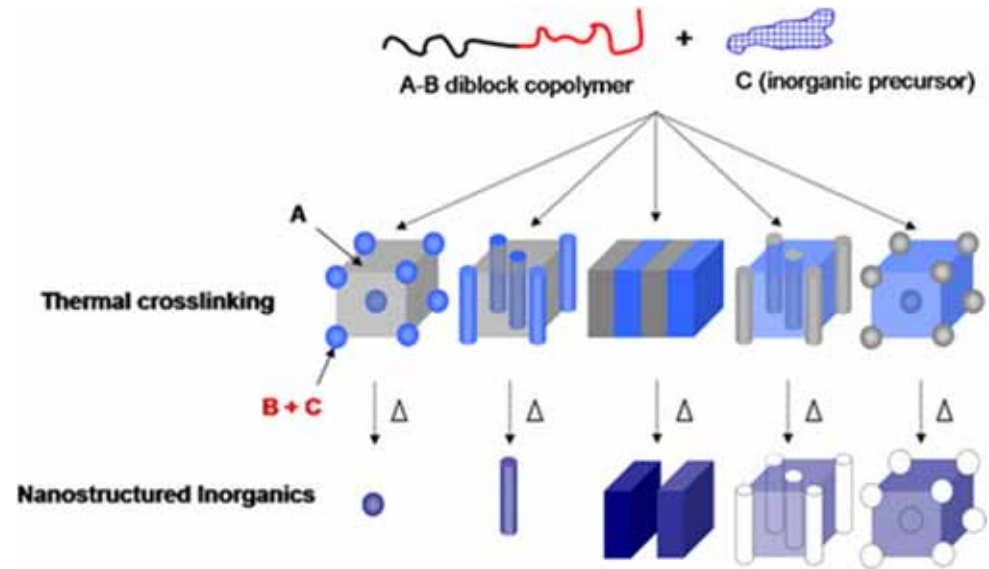
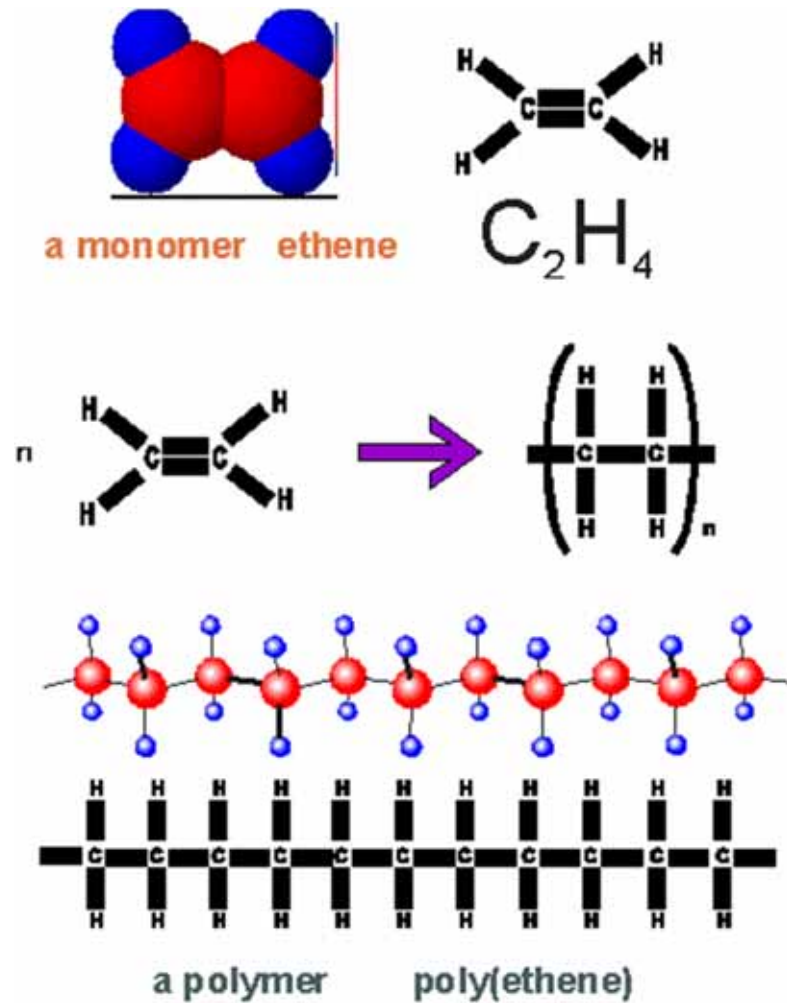


C₆₀

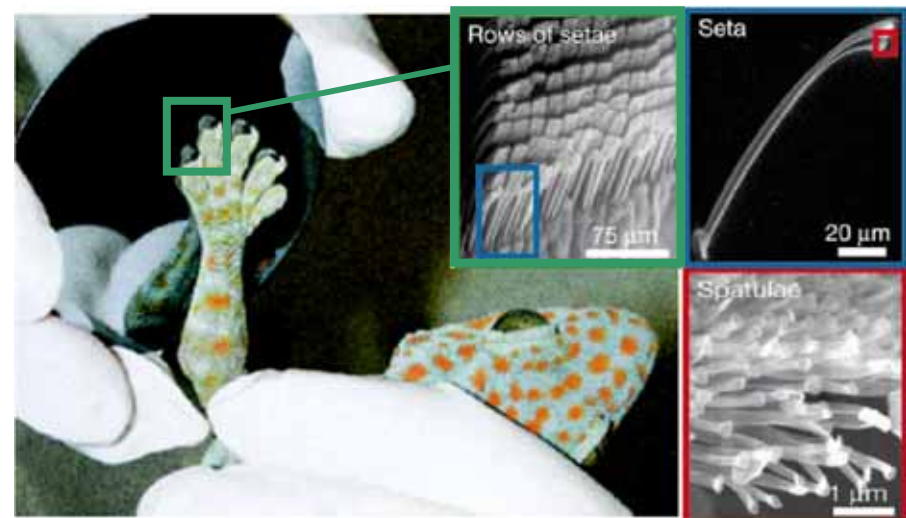
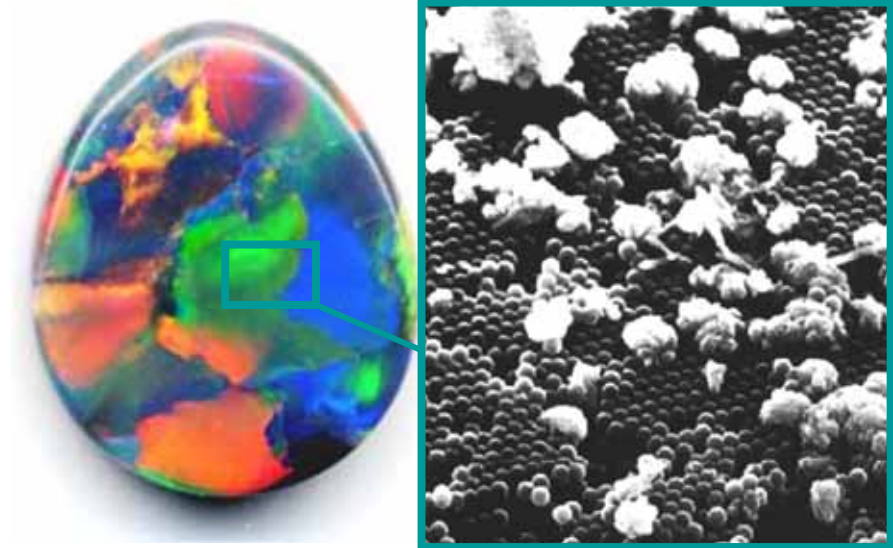
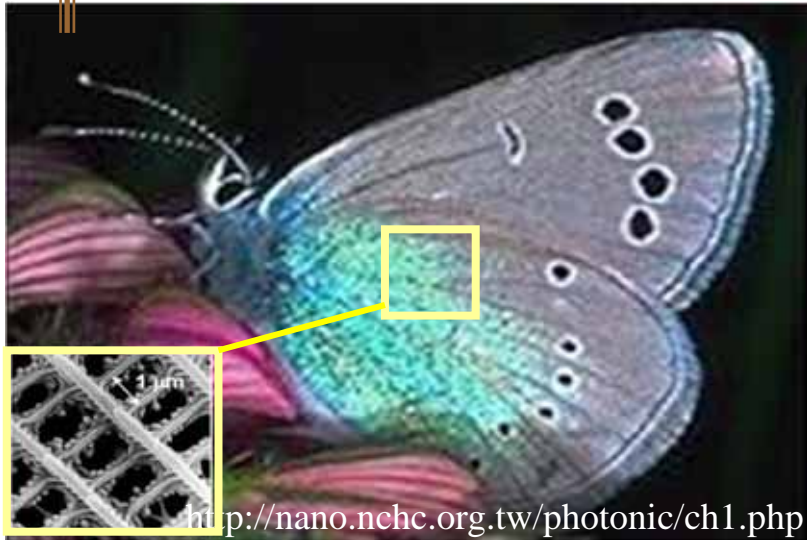


Nanodiamond
~ 2-10 nm

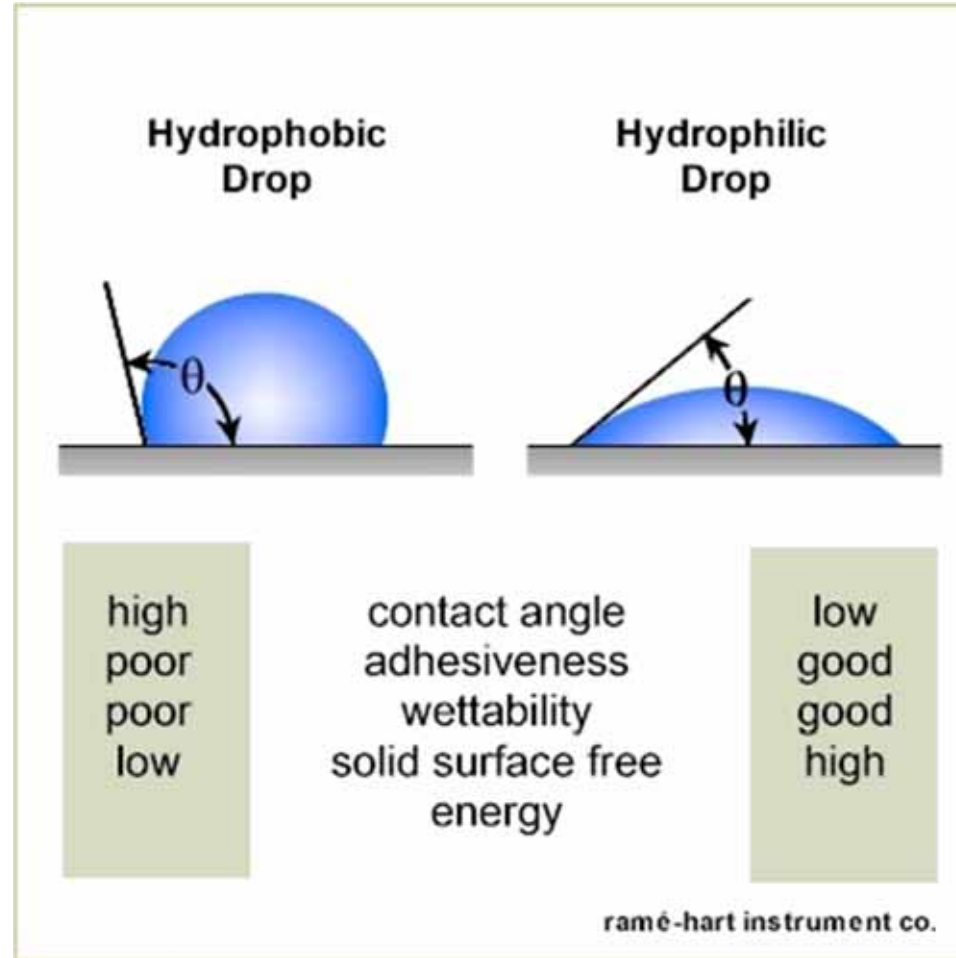
Polymer



Nature Materials

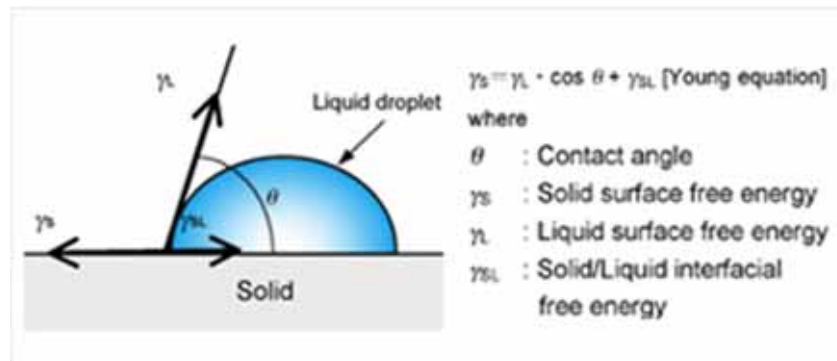


Contact Angle



Young's Equation

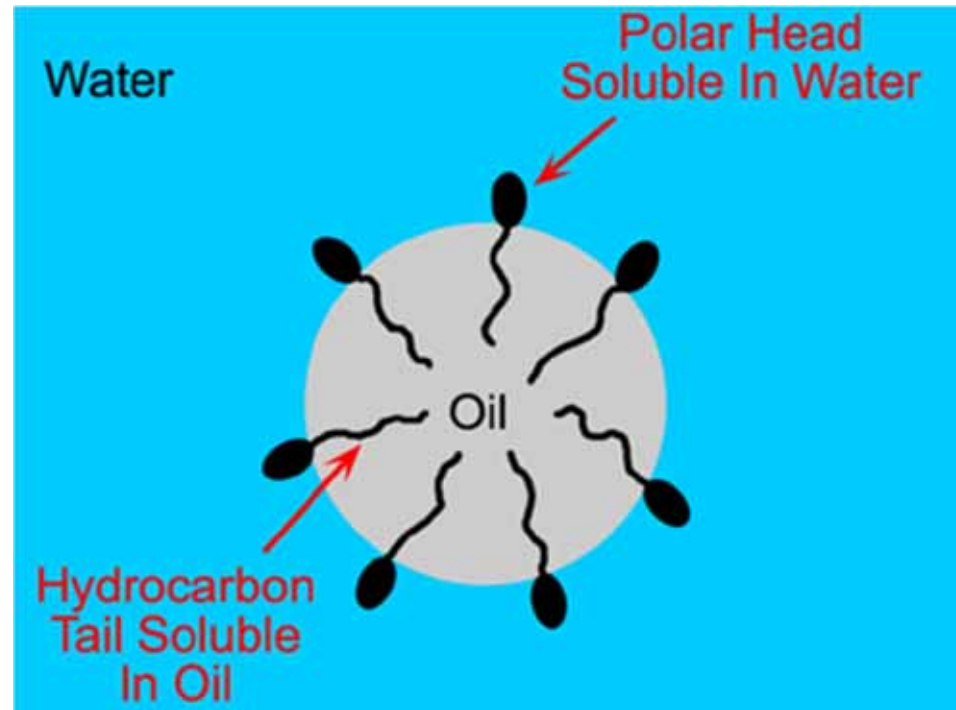
$$\gamma_{SL} + \gamma_{LV} \cos \theta_c = \gamma_{SV}$$



Surface Energy Minimization

- Surfactants
- DLVO
- Polymeric
- Nucleation
- Ostwald Ripening
- Sintering
- Restructure

Surfactant



DLVO Theory

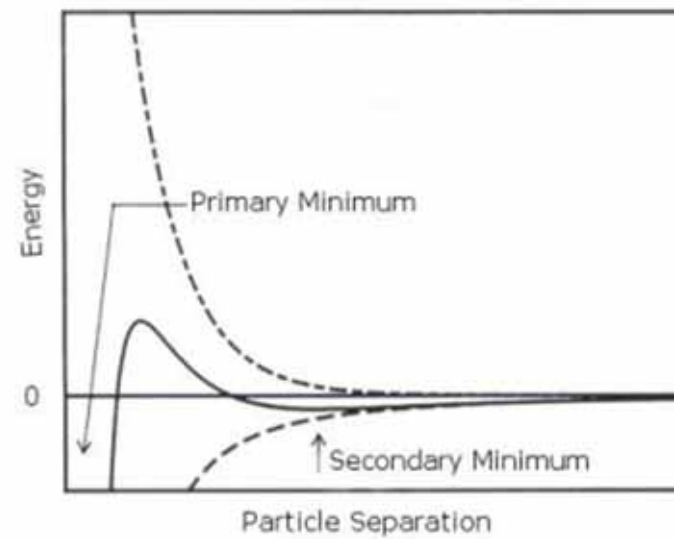
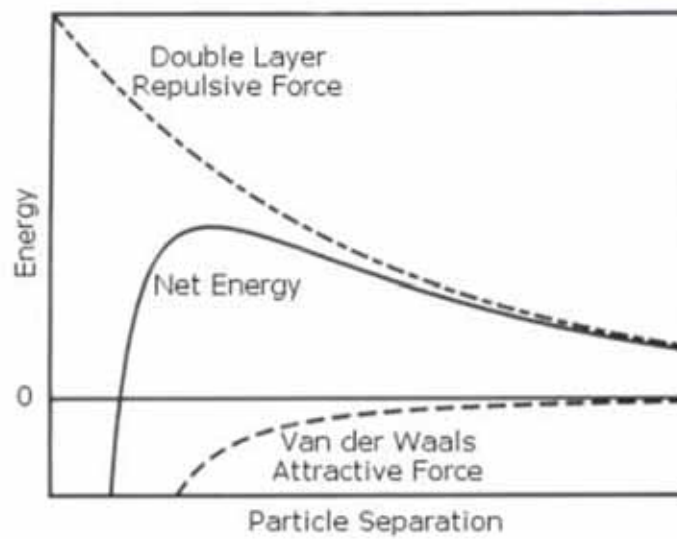
$$V_T = V_A + V_R + V_S$$

$$V_A = -A/(12 \pi D^2)$$

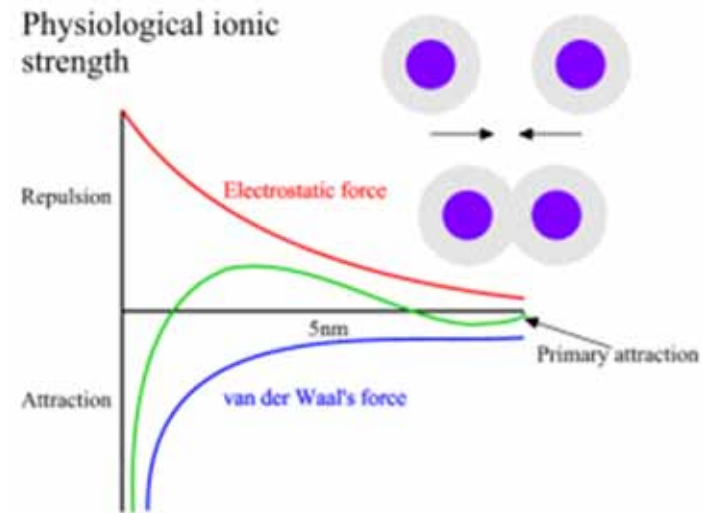
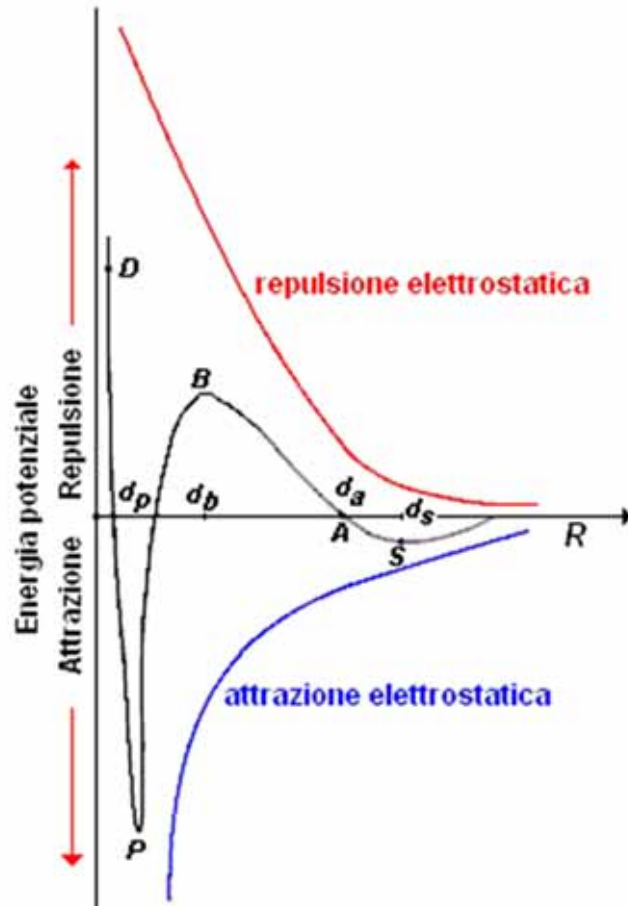
A is the Hamaker constant and D is the particle separation

$$V_R = 2 \pi \epsilon a \xi^2 \exp(-\kappa D)$$

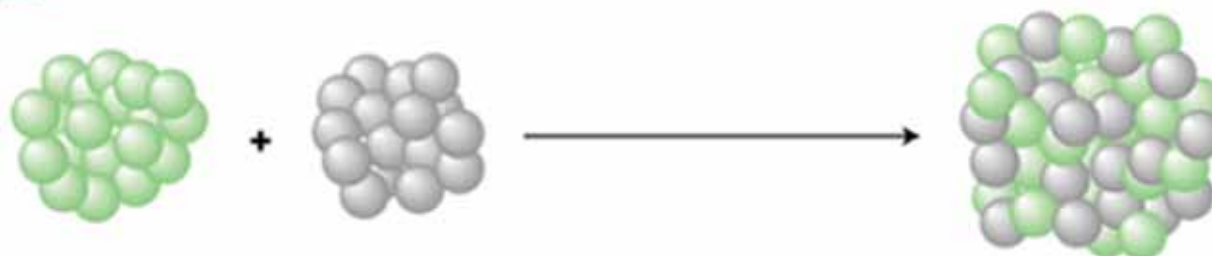
a is the particle radius, π is the solvent permeability,
 κ is a function of the ionic composition and ξ is the zeta potential



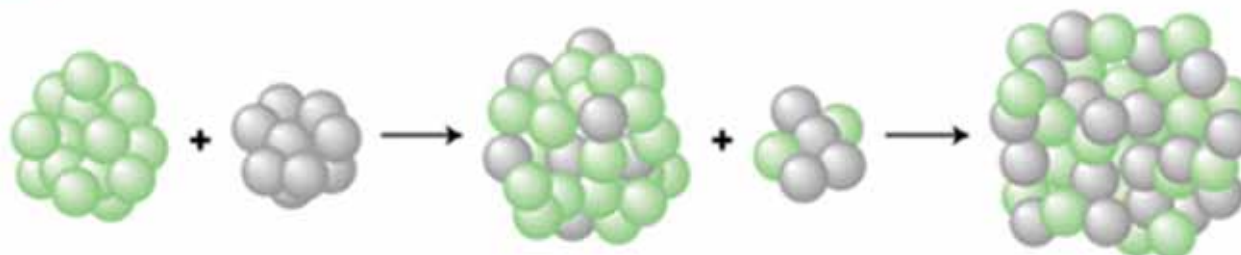
DLVO Theory



a Coalescence



b Ostwald ripening



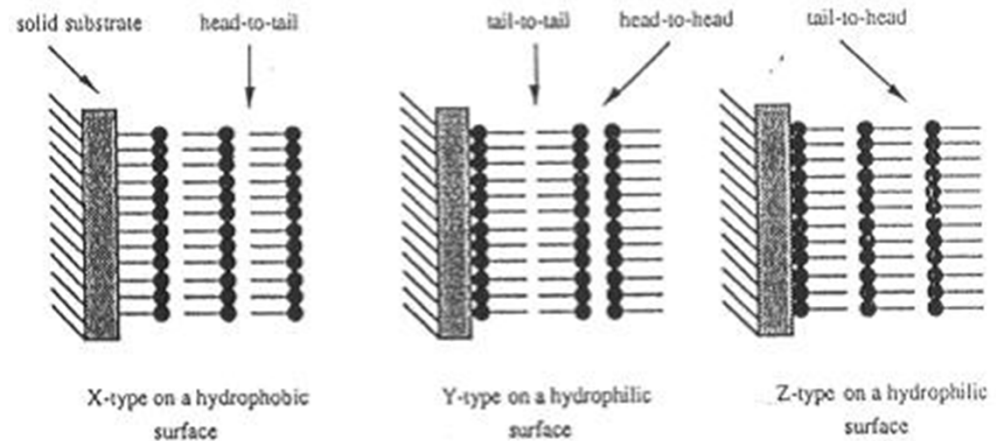
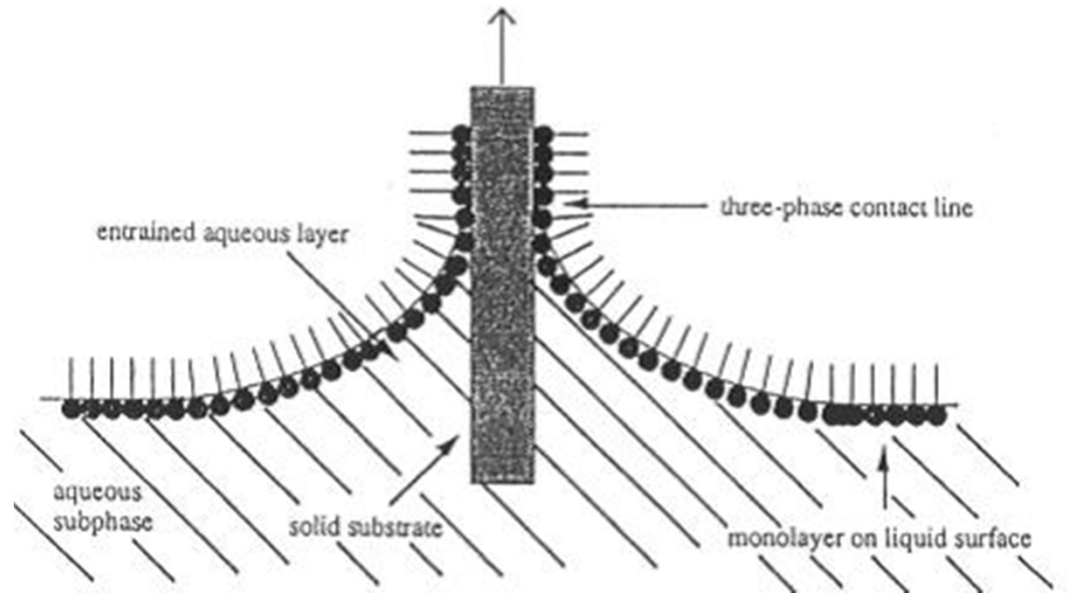
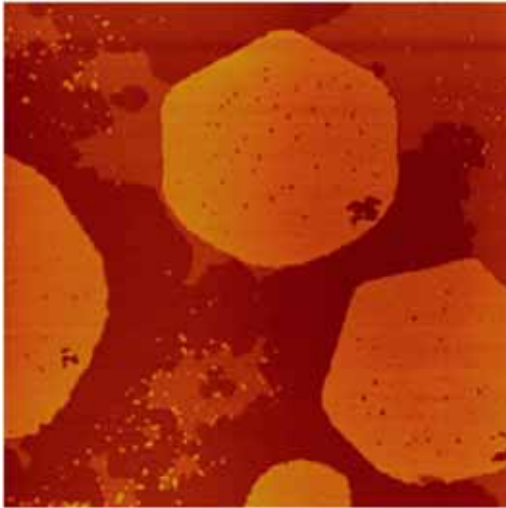
Two main mechanisms are shown here: **a**, coalescence sintering, and **b**, Ostwald ripening sintering. Coalescence sintering occurs when two clusters touch or collide and merge to form one bigger cluster. In contrast, Ostwald ripening sintering occurs by evaporation of atoms from one cluster, which then transfer to another. This is a dynamic process — both clusters exchange atoms, but the rate of loss from the smaller cluster is higher, because of the lower average coordination of atoms at the surface and their relative ease of removal. Thus big clusters get bigger at the expense of smaller clusters, which shrink and eventually disappear. The latter process is the usual form of sintering for metal clusters on a supported surface that are well spaced apart, although coalescence can occur for a high density of clusters. In general, the presence of the surface results in SMORS (surface-mediated Ostwald ripening sintering) in which material is transferred from one cluster to another by diffusion across the surface, and not through the gas phase.

Synthesis of Nanoparticles and Surface Modifications

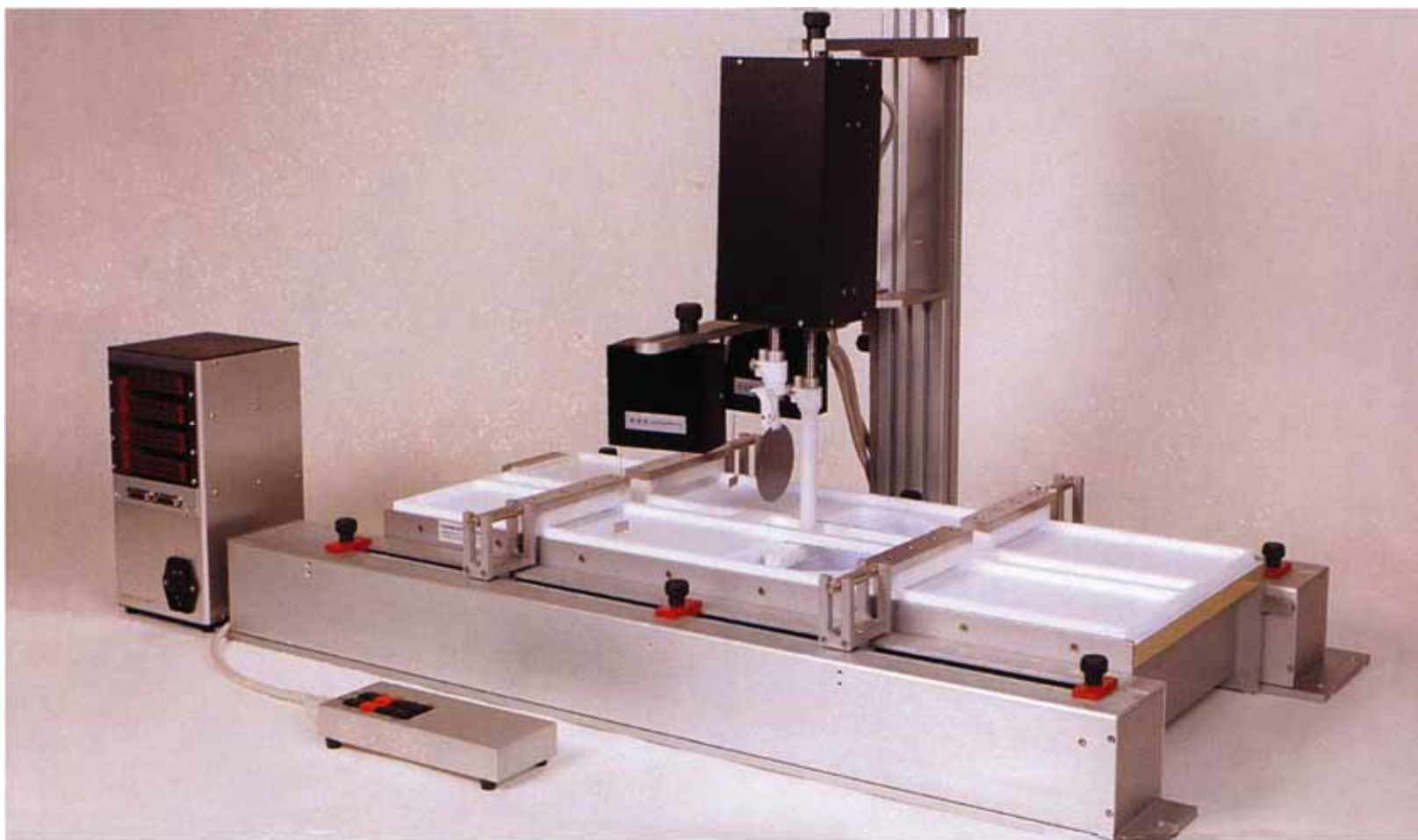
Self-Assembly

- Static assembly
- Dynamic assembly
 - $RT = 8.314 \text{ J/mol} \times 300 = 2.4 \text{ kJ/mol}$
- Driving forces
 - Chemisorption
 - Surface effect
 - Hydrophobic-hydrophilic
 - Intermolecular forces
 - Capillary force

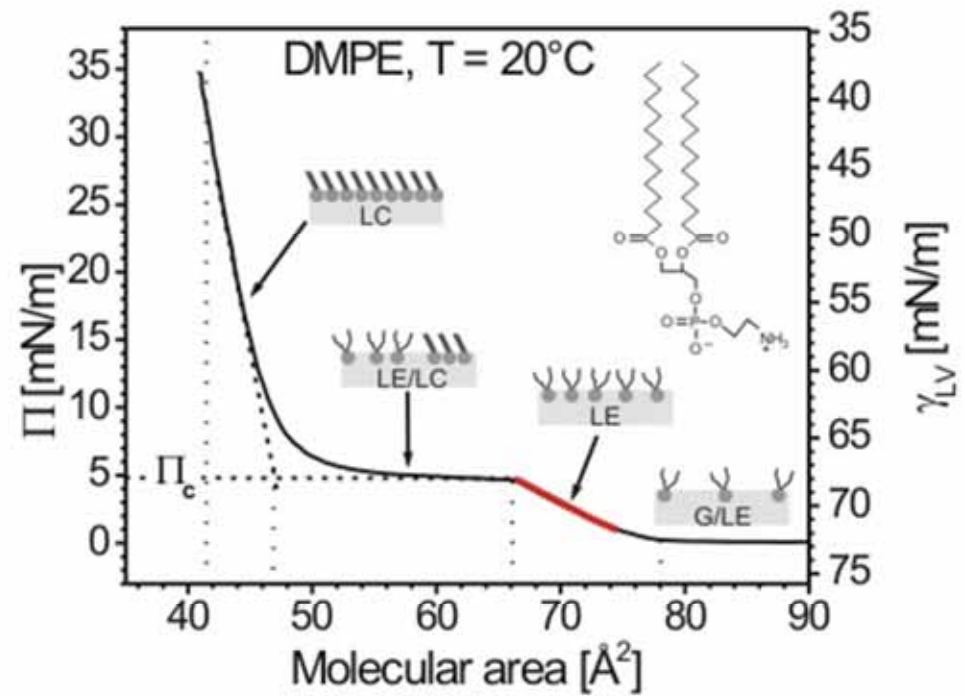
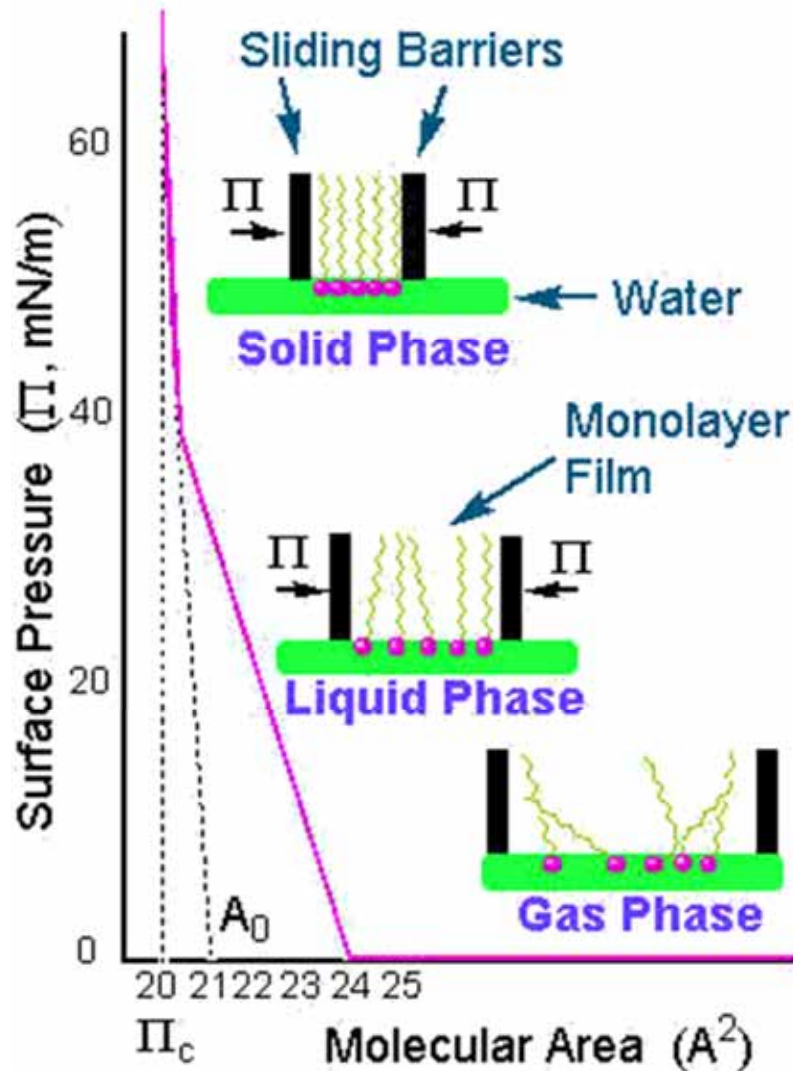
Langmuir-Blodgett Films



Langmuir-Blodgett Films

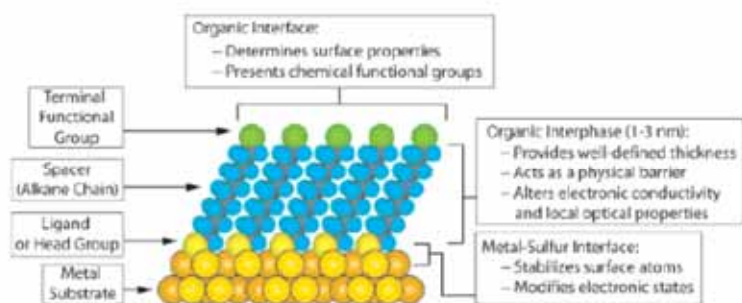


Isotherm



Self-Assemble Monolayer (SAM)

Chem. Rev. 2005, 105, 1103–1169



S-Au 25-30 Kcal/mole
Si-O 190 kcal/mole

Morphology of Substrate				Morphology of Substrate			
Ligand	Substrates	Thin Films or Bulk Material	Nanoparticles or Other Nanostructures	Ligand	Substrates	Thin Films or Bulk Material	Nanoparticles or Other Nanostructures
ROH	Fe ₂ O ₃	36	35	RSSR'	Ag	89	90
	Si-H	37			Au	20	90-92
	Si				CdS		61
RCOO-RCOOH	α-Al ₂ O ₃	38,39		R-S-S	Pd	30	
	Fe ₂ O ₃		40		Au	93	
	Ni		41,42				
	Ti/TiO ₂	43		RCSSH	Au	94	
RCOO-OCOR	Si(111):H	44			CdSe		95
	Si(100):H			RS ₂ O ₂ Na ⁺	Au	96	
Ene-diol	Fe ₂ O ₃		45		Cu	97	
RNH ₂	FeS ₂	46		RSeH	Ag	99	
	Mica	47			Au	100,101	
	Stainless Steel 316L	48			CdS		60
	YBa ₂ Cu ₃ O _{7-δ}	49	50	RSeSeR'	CdSe		102
RCaN	CdSe				Au	101	
	Ag	51		R ₃ P	Au		103
R-N=N'(BF ₄)	Au				FeS ₂	46	
	GaAs(100)	52			CdS		104
	Pd	52			CdSe		104
RSH	Si(111):H	52			CdTe		104
	Ag	26	53,54	R ₃ P=O	Co		105,106
	Ag ₂ Ni ₁₀	55			CdS		104
	AgS		56		CdSe		104
	Au	26	57		CdTe		104
	AuAg		58	RPO ₃ ²⁻ /RPO ₃ (OH) ₂	Al	107	
	AuCu		58		Al-OH	108	
	Au ₂ PH ₄		58		Ca ₁₀ (PO ₄) ₆ CO ₃ (OH) ₂	109	
	CdTe		59		GaAs	110	
	CdSe		60		GaN	110	
	CdS		61,62		Indium tin oxide	111	
	Cu	26	58		(ITO)		
	FePt		63-66		Mica	112	
	GaAs	67			TiO ₂	113,114	
	Ge	68			ZrO ₂	114,115	
	Hg	69-71		RPO ₄ ³⁻	CdSe		116-118
	HgTe		72		CdTe		118,119
	InP	73			Al ₂ O ₃	120	
	Ir		74		Nb ₂ O ₅	120	
	Ni	75			Ta ₂ O ₅	121	
RNaC	PbS		76-78	RNaC	Pt	123	124
	Pd	30	74,79		Si	37	
	PdAg		58		Si(111):H	125	
	Pt	32	80				
	Ru		81	RSX ₃ X = H, Cl, OCH ₂ CH ₃	HfO ₂	126	
	Stainless Steel 316L	48			ITO	127	
	YBa ₂ Cu ₃ O _{7-δ}	82			PtO	128	
	Zn	83			TiO ₂	113,126,129	
	ZnSe	84			ZrO ₂	126,129	
	ZnS		85				
RSAc	Au	86					
	Au		87				
R-SR'	Au	88					

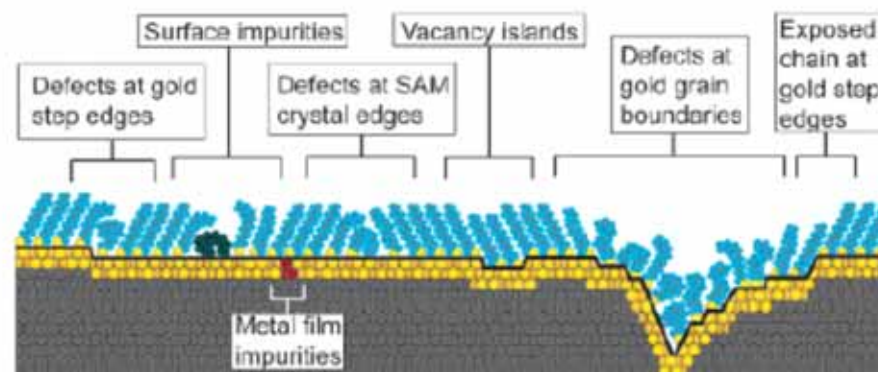
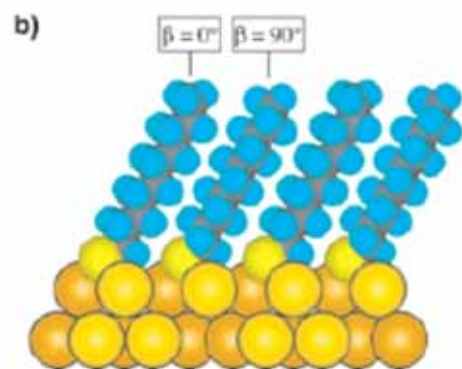
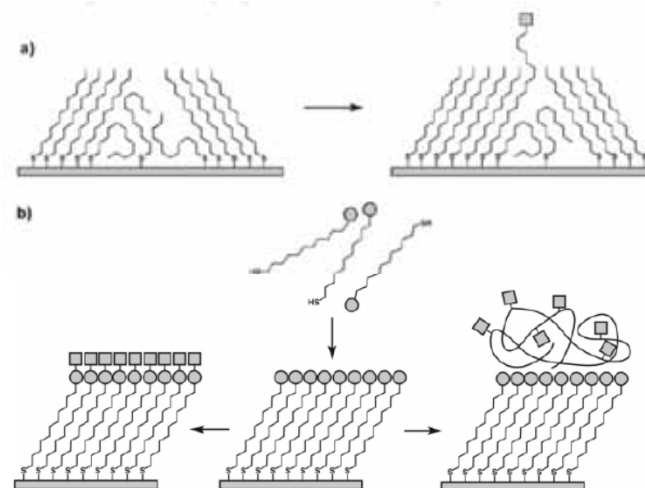
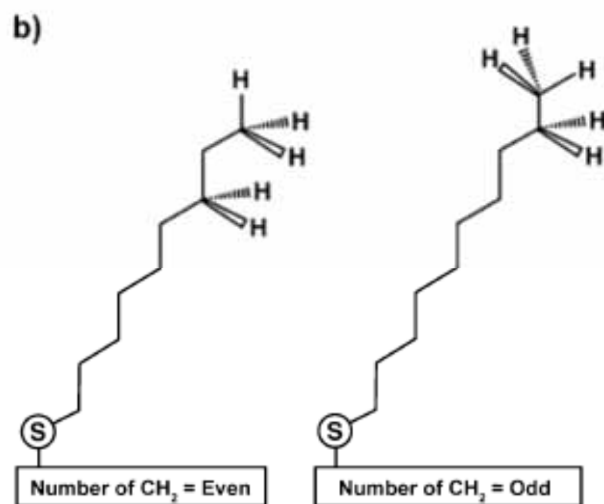


Figure 7. Schematic illustration of some of the intrinsic and extrinsic defects found in SAMs formed on polycrystalline substrates. The dark line at the metal–sulfur interface is a visual guide for the reader and indicates the changing topography of the substrate itself.



^a (a) Insertion of a functional adsorbate at a defect site in a preformed SAM. (b) Transformation of a SAM with exposed functional groups (circles) by either chemical reaction or adsorption of another material.

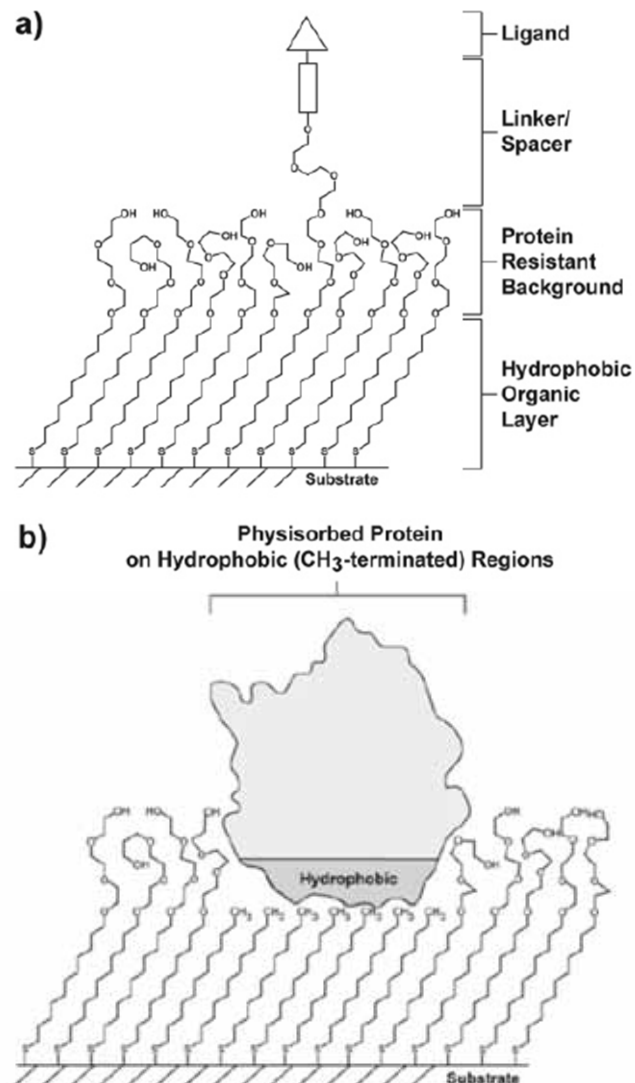


Figure 21. Schematic illustrations of (a) a mixed SAM and (b) a patterned SAM. Both types are used for applications in biology and biochemistry.

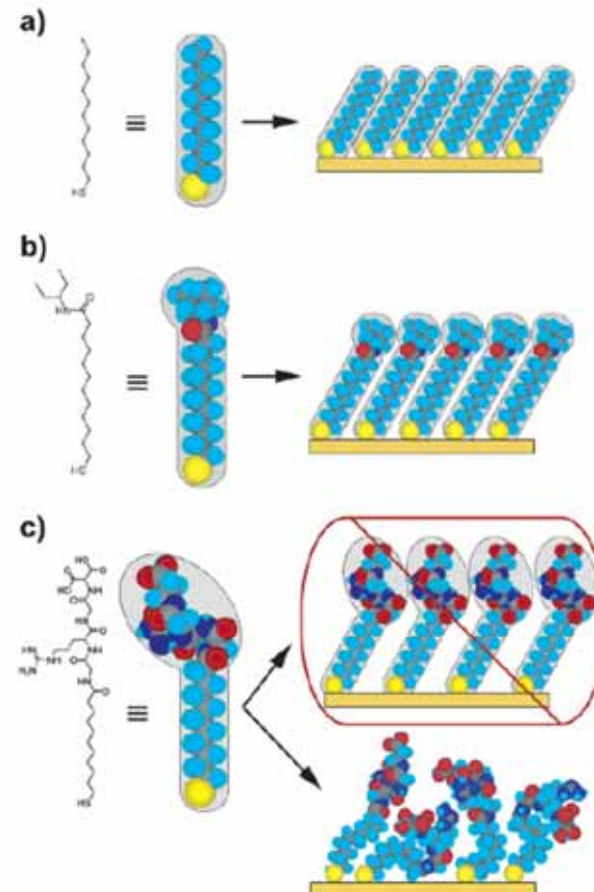


Figure 22. Schematic diagram illustrating the effects that large terminal groups have on the packing density and organization of SAMs. (a) Small terminal groups such as $-\text{CH}_3$, $-\text{CN}$, etc., do not distort the secondary organization of the organic layer and have no effect on the sulfur arrangement. (b) Slightly larger groups (like the branched amide shown here) begin to distort the organization of the organic layer, but the strongly favorable energetics of metal-sulfur binding drive a highly dense arrangement of adsorbates. (c) Large terminal groups (peptides, proteins, antibodies) sterically are unable to adopt a secondary organization similar to that for alkanethiols with small terminal groups. The resulting structures probably are more disordered and less dense than those formed with the types of molecules in a and b.

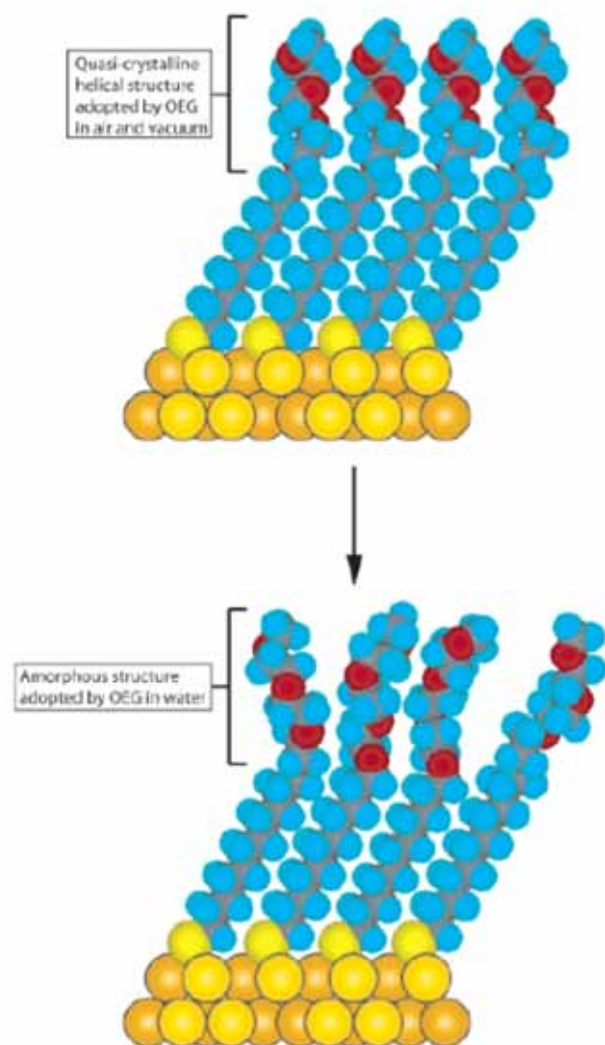
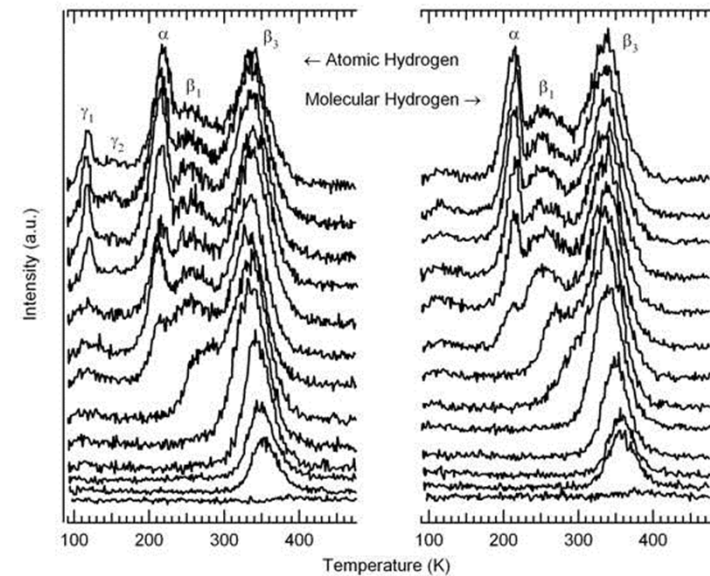


Figure 23. Schematic illustration of the order–disorder transition evidenced by SAMs of alkanethiolates terminated with triethylene glycol. The EG₃ group loses conformational ordering upon solvation in water.

Temperature Programmed Desorption

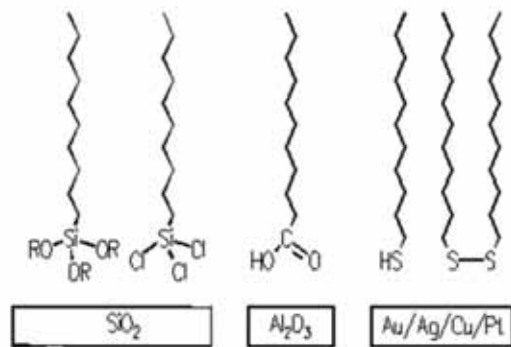


Self-Assembly

- Substrates
- Interstitial adhesion layer
- Noble metal layer
- Organo-sulfur

Organosilanes

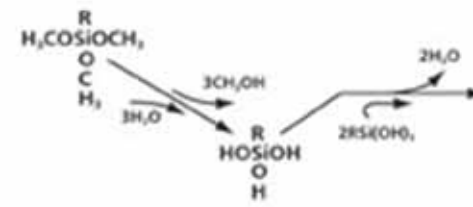
Self-assembled monolayers



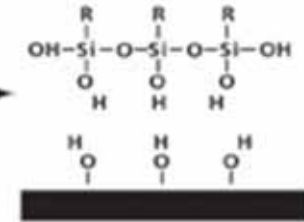
Immersion of substrate in a solution containing the adequate molecules for 12 - 24 hours yields an ordered monolayer

- Surface
- silicon oxide: silanisation
- aluminum oxide: fatty acids
- metals: thiols and sulfides

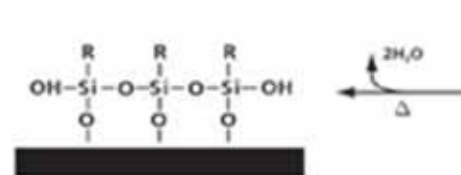
Hydrolysis (1)



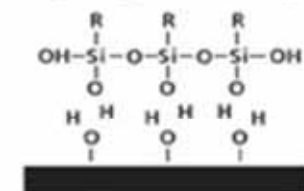
Condensation of Oligomers (2)



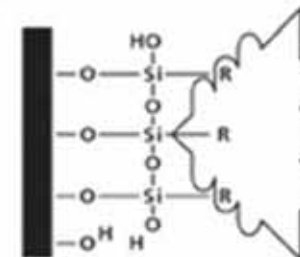
Bond Formation (4)



Hydrogen Bonding (3)

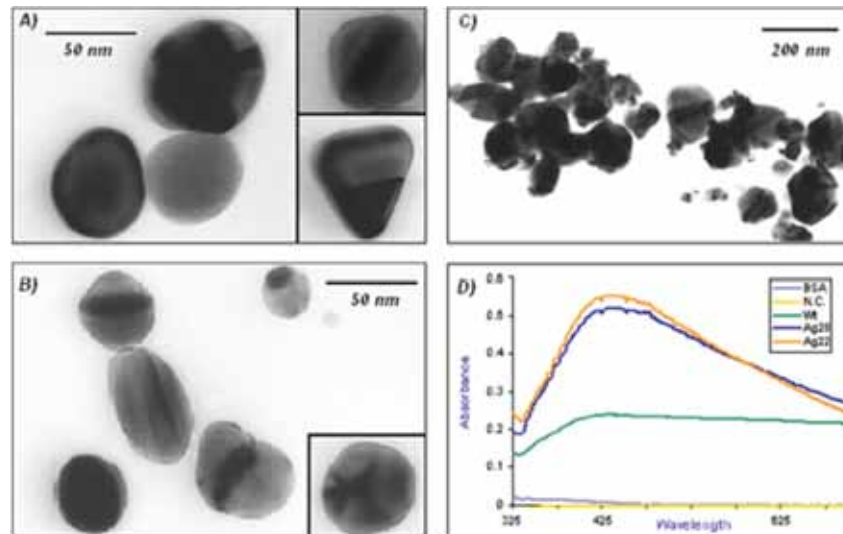
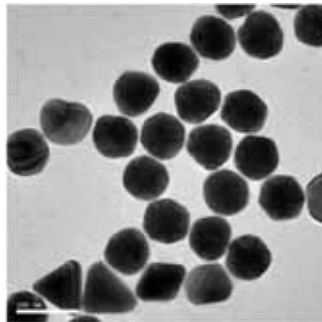
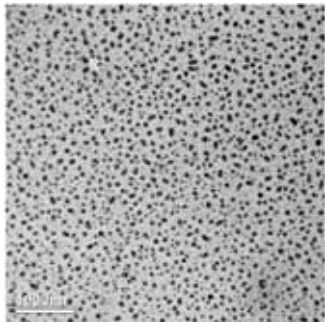
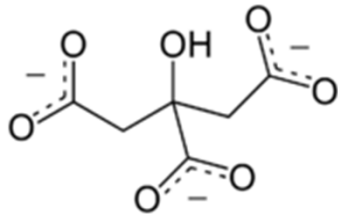


Reaction and bond formation of the R group (5)



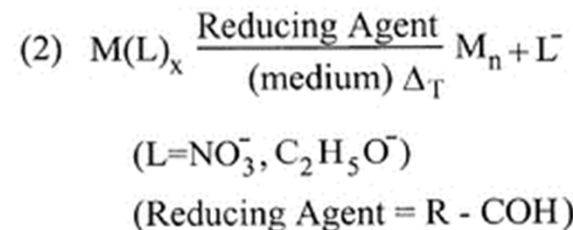
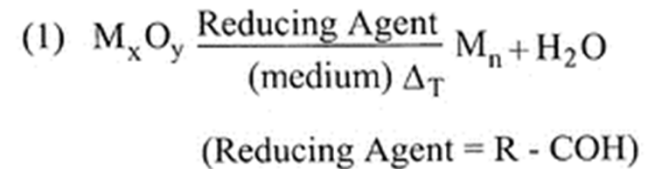
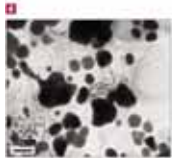
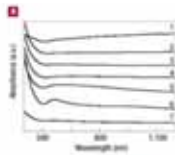
Synthesis of Silver Nanoparticles

1. ***A solution of AgNO_3 ($1.0 \times 10^{-3} \text{ M}$) in deionized water was heated until it began to boil.***
2. ***Sodium citrate solution was added dropwise to the silver nitrate solution as soon as the boiling commenced. The color of the solution slowly turned into grayish yellow, indicating the reduction of the Ag^+ ions.***
3. ***Heating was continued for an additional 15 min, and then the solution was cooled to room temperature before employing for further experimentation.***



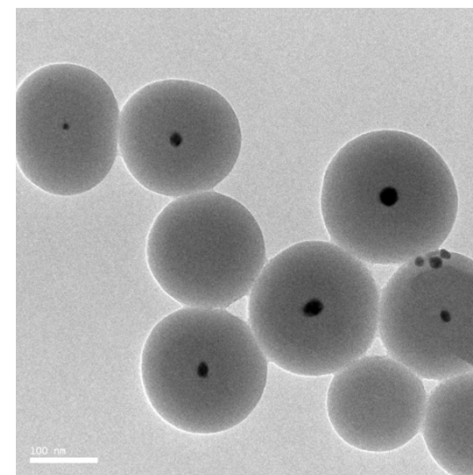
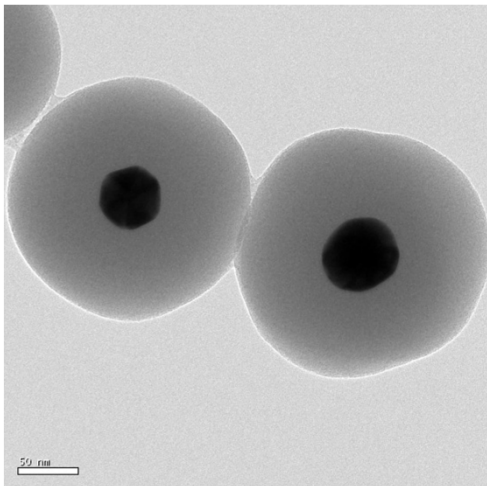
Synthesis of Gold Nanoparticles

1. Add 20 mL of 1.0 mM HAuCl_4 to a 50 mL round bottom flask on a stirring hot plate.
2. Add a magnetic stir bar and bring the solution to a boil.
3. To the boiling solution, add 2 mL of a 1% solution of trisodium citrate dihydrate
4. The gold sol gradually forms as the citrate reduces the gold(III). Stop heating when a deep red color is obtained.

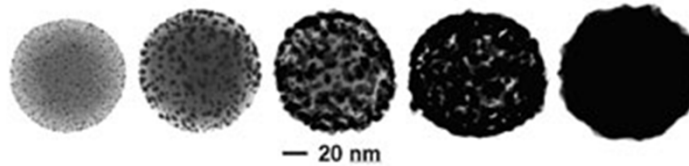
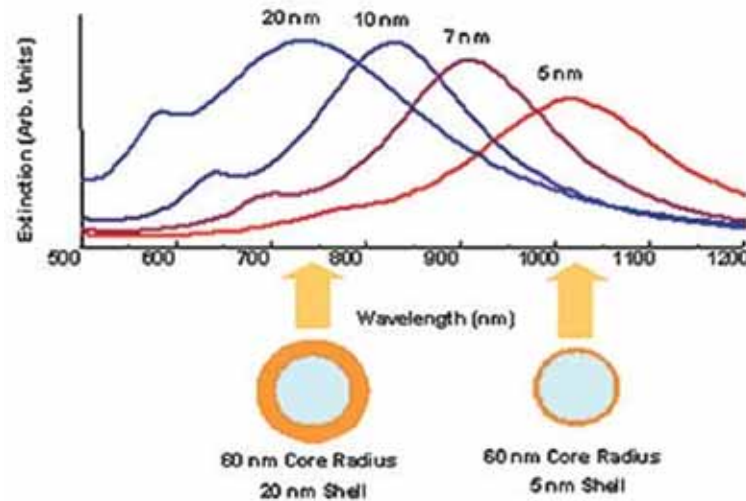


Construction of Core Shell Ag/Au@SiO₂ Nanoparticles

1. *Under vigorous stirring, 1 ml of the silver/ gold colloids solution was mixed with 250 mL of isopropanol and 25 mL of deionized water.*
2. *Immediately after the addition of 4 mL of 30% ammonium hydroxide, different amounts of tetraethoxysilane (TEOS) were added to the reaction mixture.*
3. *To obtain different silica layer thicknesses, TEOS solutions with a concentration between 50% and 100% was added to the suspension. The reaction was stirred at room temperature for 30 minutes and then was allowed to age without agitation at 4°C overnight.*
4. *Each suspension of silica-coated silver/gold nanoparticles was washed and centrifuged, followed by re-suspension in water. The thickness of the silica layers was determined from TEM images .*



Core-Shell Nanoparticles



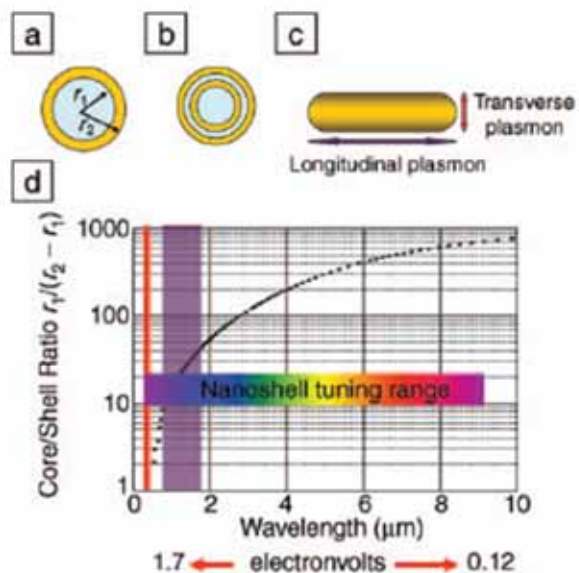


Figure 1. (a) Schematic illustration of a silica-core, gold-shell nanoshell, indicating inner (r_1) and outer (r_2) radii of the shell layers. (b) Depiction of a four-layer, concentric nanoshell. (c) Schematic illustration of a metallic nanorod. (d) Plot of nanoshell resonance as a function of core and shell dimensions, overlaid with reported spectral ranges of nanorod resonances (red, transverse plasmon; purple, longitudinal plasmon), and reported nanoshell and concentric nanoshell combined spectral range of plasmon response.

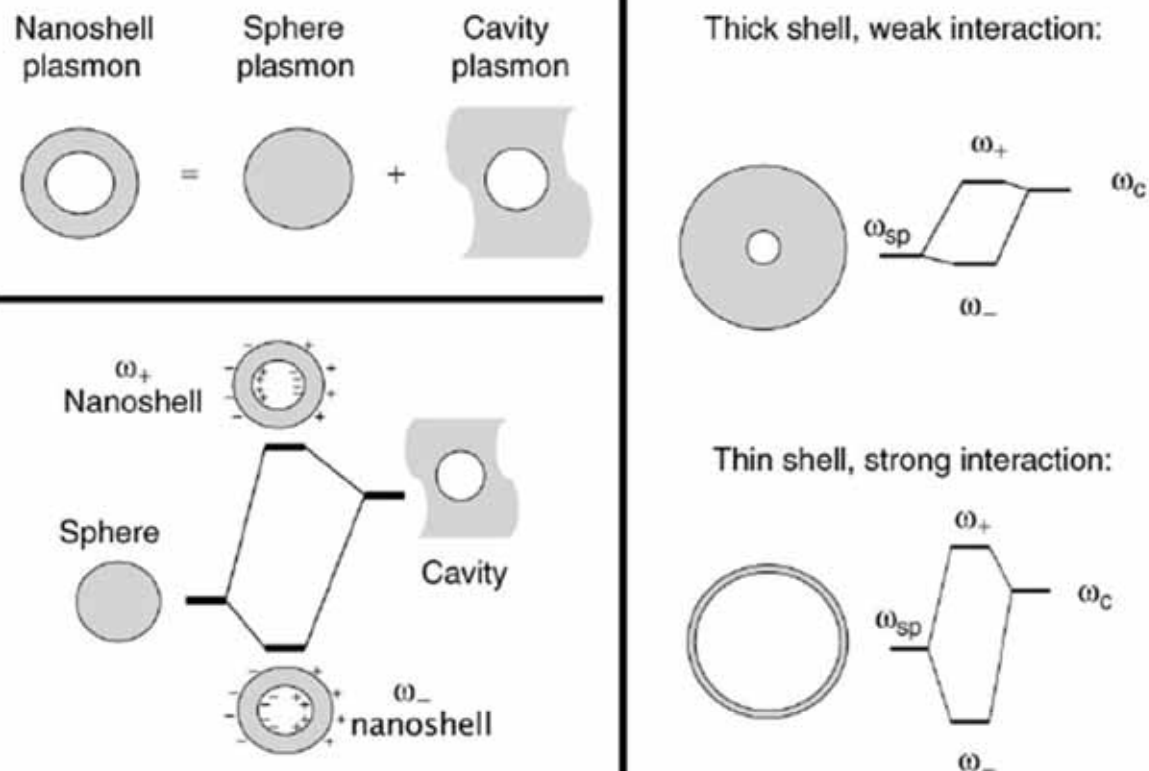


Figure 2. Plasmon hybridization and the sphere-cavity model for nanoshells: the interaction between a sphere (resonance frequency, ω_{sp}) and a cavity plasmon (resonance frequency, ω_c) is tuned by varying the thickness of the shell layer of the nanoparticle. Two hybrid plasmon resonances, the ω_- "bright," or "bonding," plasmon and the ω_+ "dark," or "anti-bonding," plasmon resonances are formed. The lower-energy plasmon couples most strongly to the optical field.

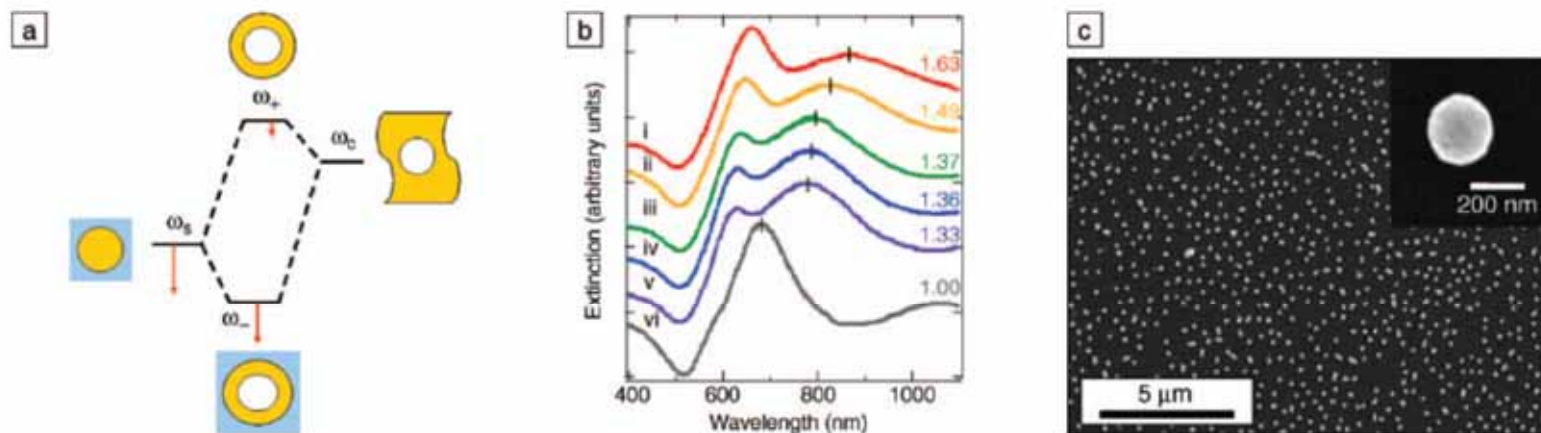


Figure 5. (a) Plasmon hybridization picture applied to surface plasmon resonance sensing with nanoshells: the low-energy “bonding” plasmon, ω_- , is sensitized to changes in its dielectric environment. The blue background schematically denotes the embedding medium for the nanoparticle. (b) Experimental curves showing plasmon resonance shifts for nanoshell-coated films in various media: (i) carbon disulfide, (ii) toluene, (iii) hexane, (iv) ethanol, (v) H₂O, and (vi) air. The index of refraction for each embedding medium is noted on the far right of the spectra. Spectra are offset for clarity. (c) Scanning electron micrograph of nanoshells deposited onto a poly(vinyl pyridine) functionalized glass surface, as used to acquire data in (b). Inset: individual nanoshell.

Preparation of $\text{Fe}_3\text{O}_4@\text{Ag}/\text{Au}$

1. *To the magnetic nanoparticle suspension obtained from commercial company, add 50 ml of a solution of Au (III) salt or Ag (I) salt at concentration of 0.01–1% mmol/L , shaking for 30 minutes, allowing Au (III) or Ag (I) ion to absorb on the surface of magnetic nanoparticle sufficiently,*
 2. *Then adding 15–40 ml of reducing agent, such as hydroxylamine hydrochloride at concentration of 40 mmol/L, reacting for 5–40 minutes.*
 3. *Further adding 1–10 ml of a solution of Au (III) salt or Ag (I) salt at concentration of 0.01–1%, shaking for 10 minutes, coating a reduced layer of gold or silver on the surface of the magnetic nanoparticle, forming super-paramagnetic composite particles having core/shell structure, separating magnetically, washing repeatedly with distilled water.*
- .

Synthesis of Quantum Dots

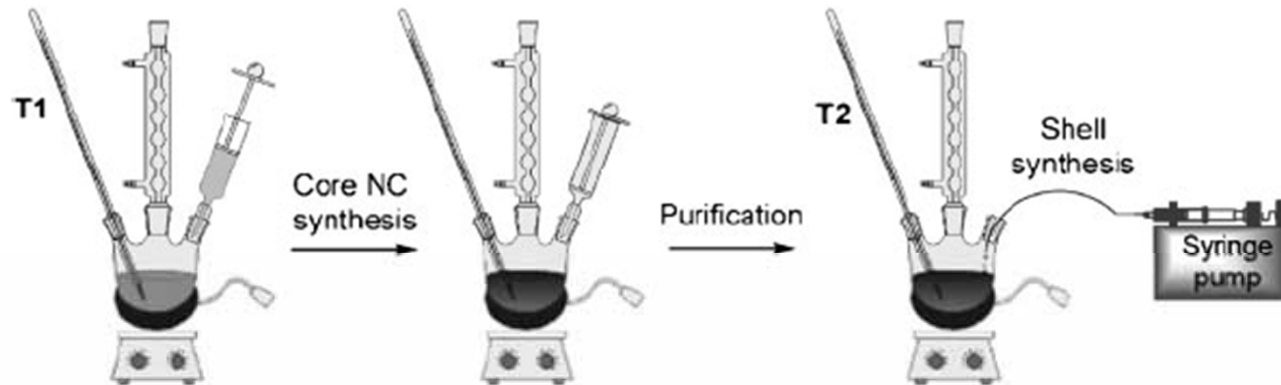
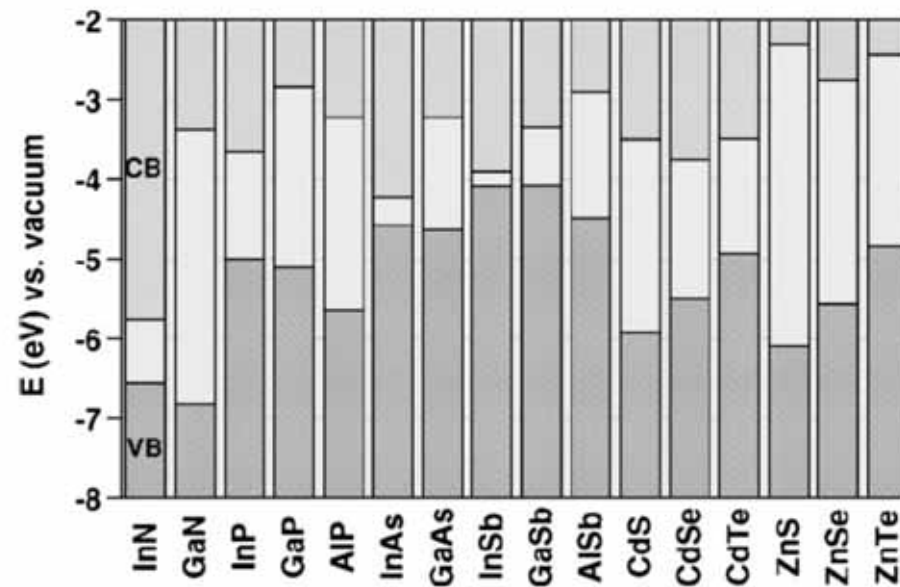


Figure 2. Two-step synthesis of core/shell nanocrystals.



Scheme 1. Electronic energy levels of selected III–V and II–VI semiconductors using the valence-band offsets from Reference [12] (VB: valence band, CB: conduction band).

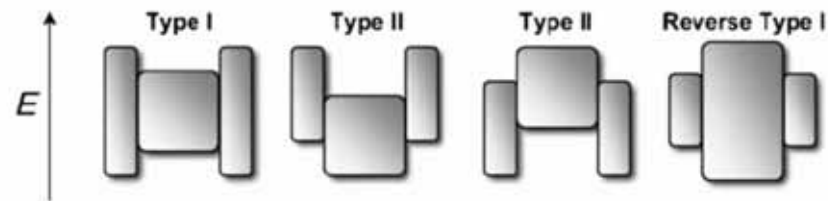
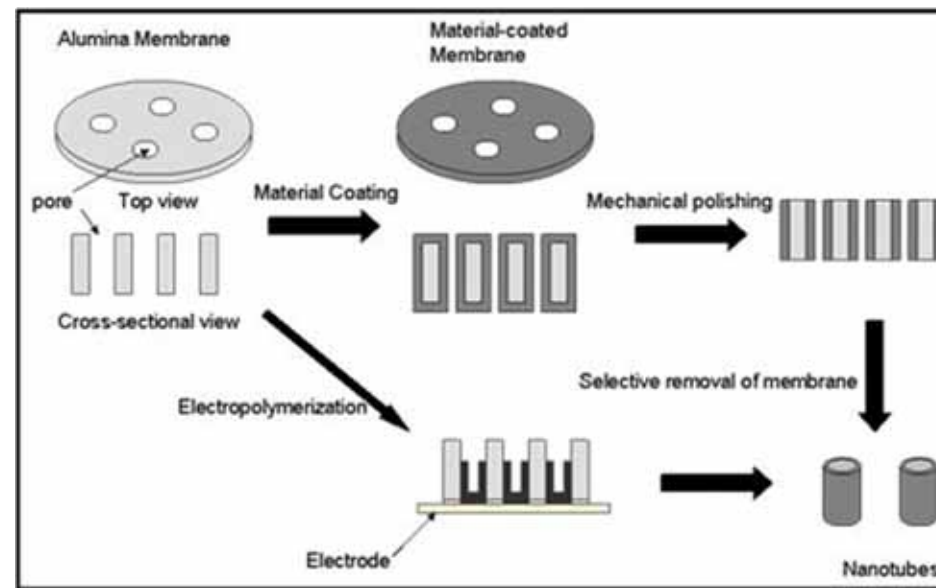


Figure 1. Schematic representation of the energy-level alignment in different core/shell systems realized with semiconductor NCs to date. The upper and lower edges of the rectangles correspond to the positions of the conduction- and valence-band edge of the core (center) and shell materials, respectively.

Template Synthesis



Porous Materials

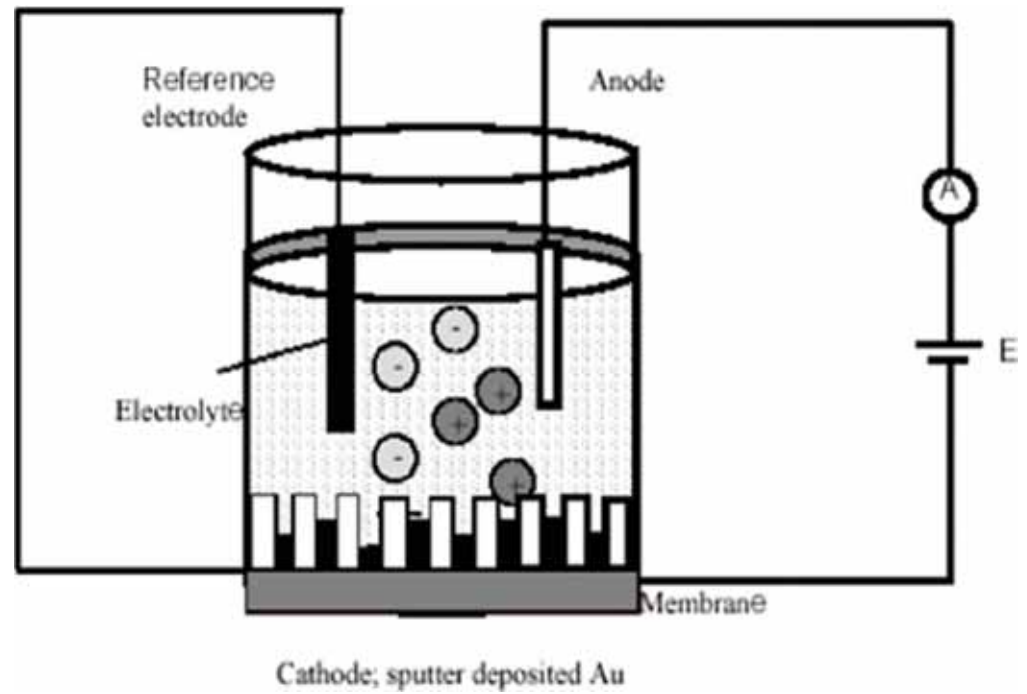
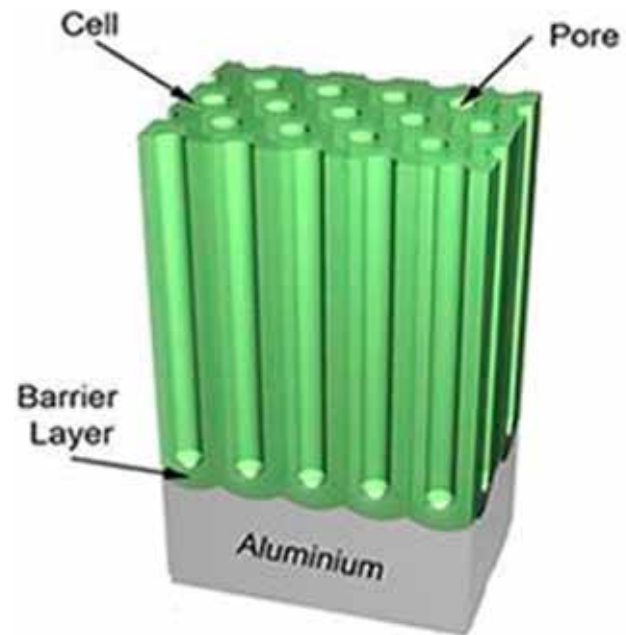
- AAO
- MCM-41

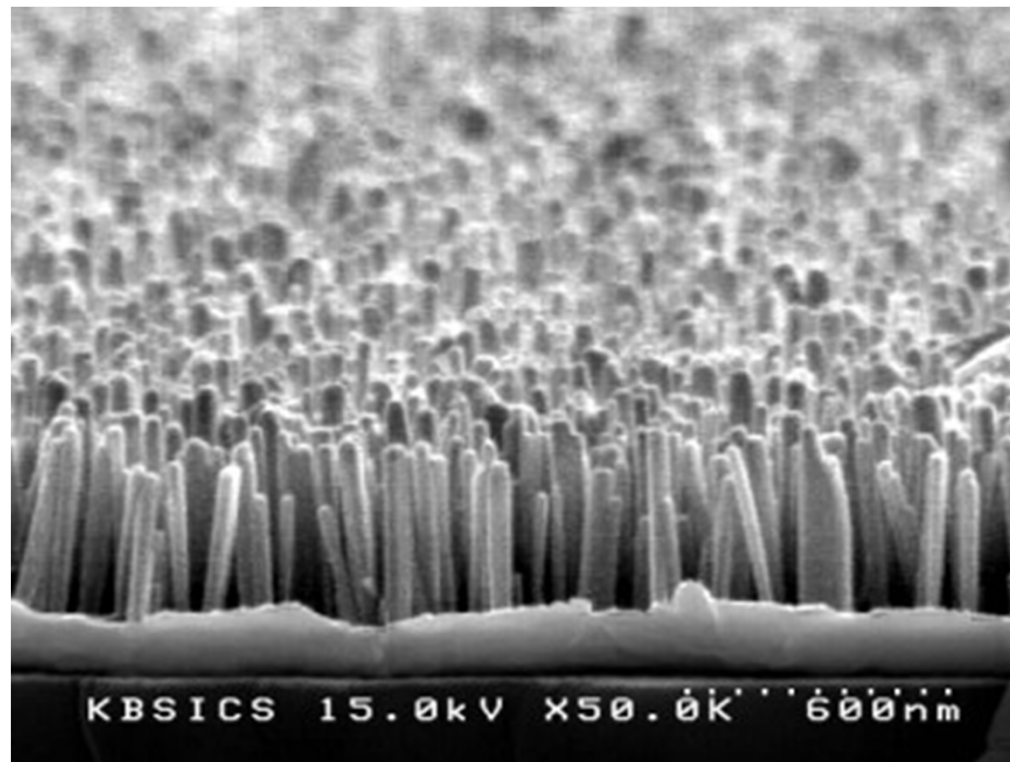
Mobil Crystalline Materials, or MCM-41

Santa Barbara Amorphous type material, or SBA-15

- Micro: $< 2\text{nm}$
- Meso:
- Macro: $> 50\text{nm}$

AAO





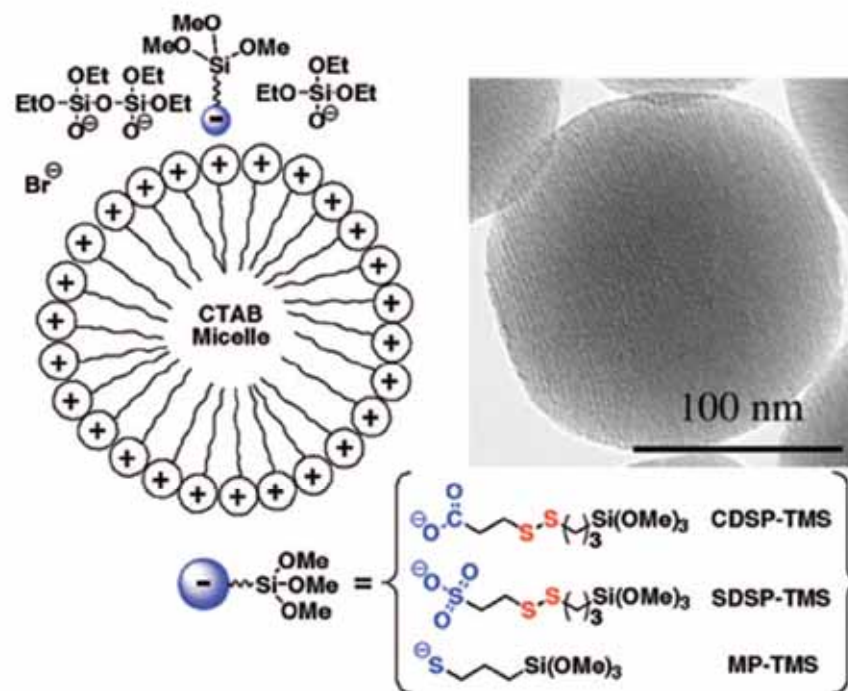


FIGURE 3. Schematic representation of the use of anionic organoalkoxysilanes for controlling the functionalization of the MSN materials. The MCM-41-type mesoporous channels are illustrated by the parallel stripes shown in the transmission electron microscopy (TEM) micrograph of the MSN-SH material. Reproduced with permission from ref 15. Copyright 2005, Royal Society of Chemistry.

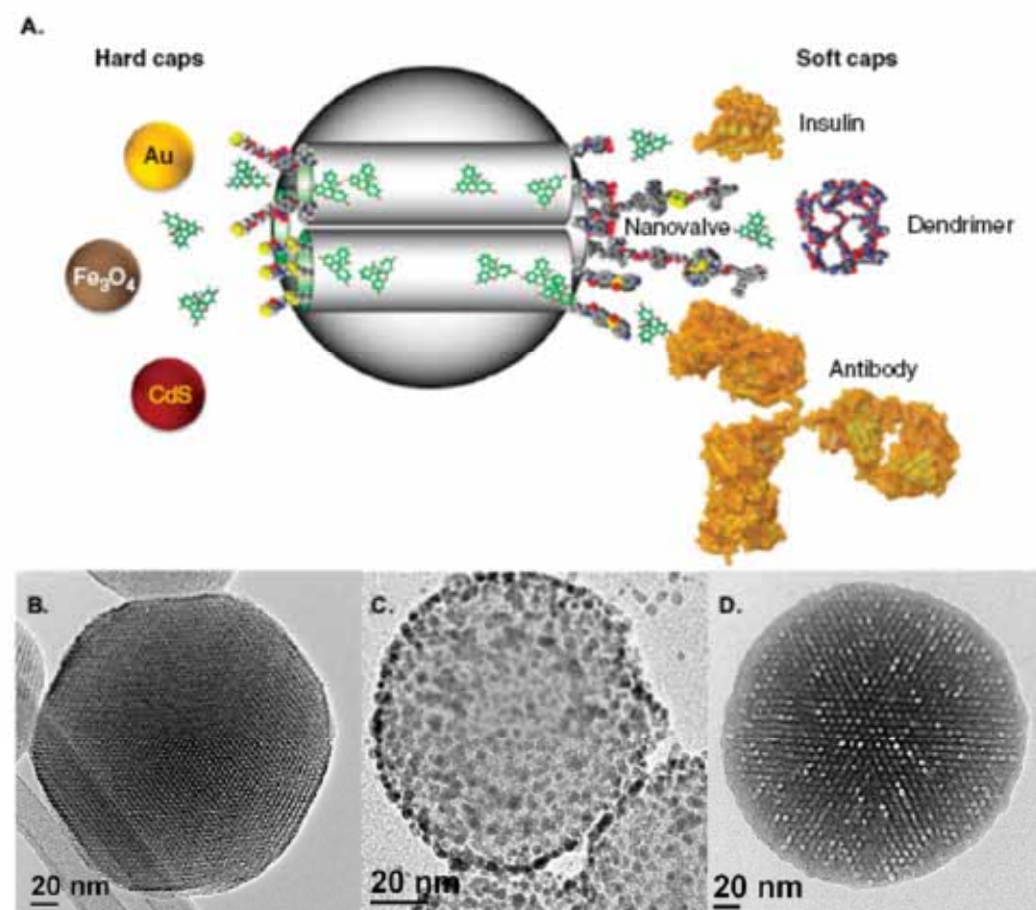


Figure 1. A. Schematic representation of a MSN loaded with drugs and capped with hard caps and soft caps highlighted in this review. Transmission electron microscopy images of (B) a MSN along the axis of the mesopores, (C) capped with hard (Au NP) and (D) with soft (polymer) caps.
MSN: Mesoporous silica nanoparticle.

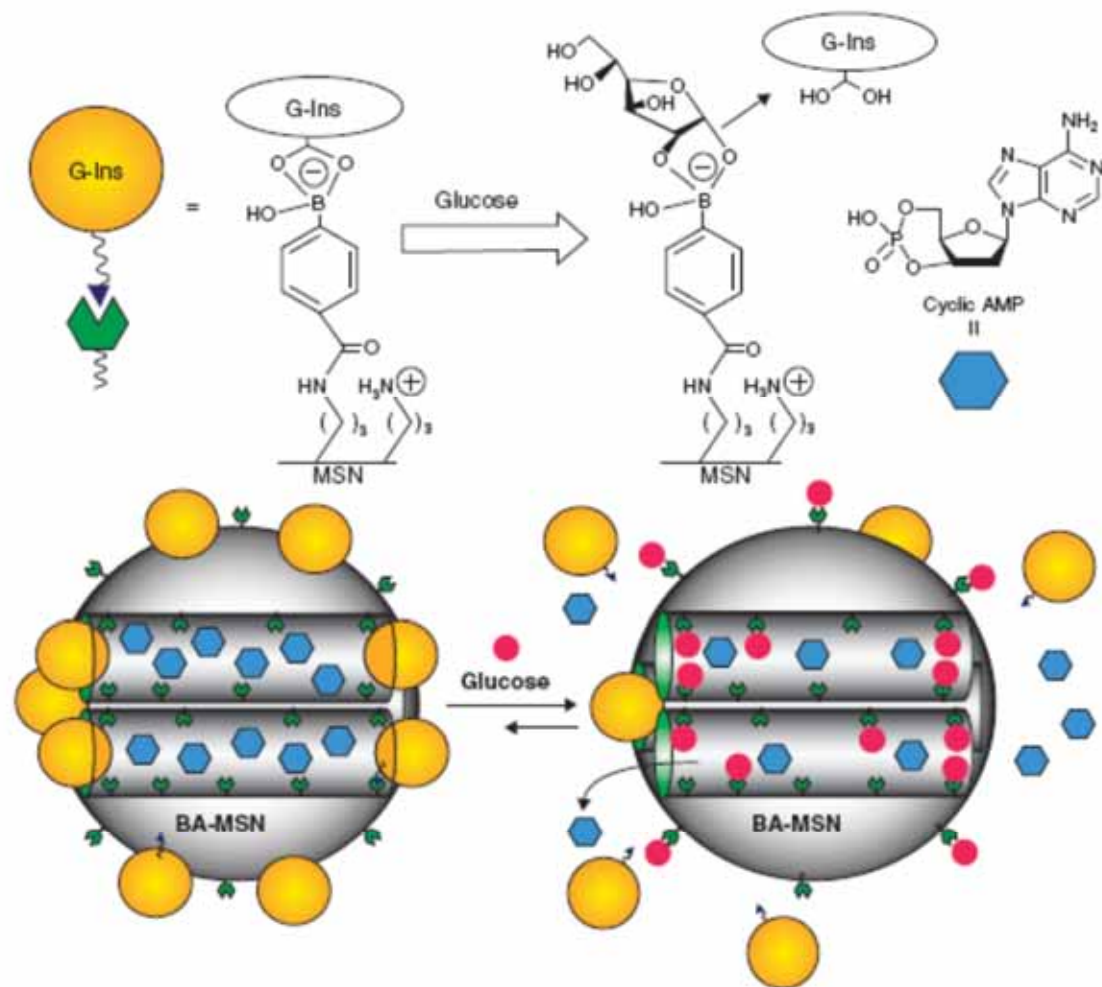
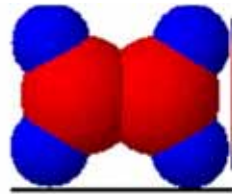


Figure 5. Schematic representation of the glucose-responsive MSN-based double delivery system for controlled release of bioactive G-Ins and cyclic AMP. The controlled release mechanism was achieved by means of the displacement reaction between blood glucose and G-Ins based on reversible boronic acid-diol complexation. High glucose concentration triggers the G-Ins uncapping and the release of cyclic AMP sequentially to diminish the higher than normal level of blood glucose.

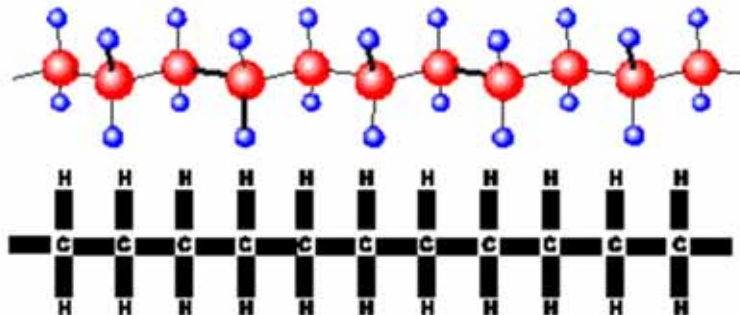
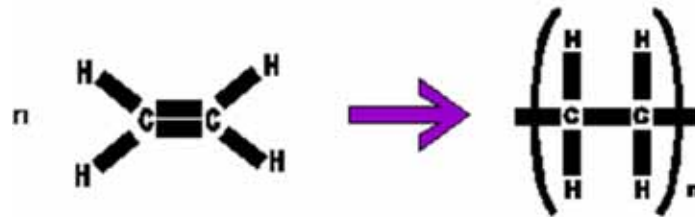
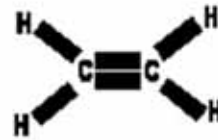
Reproduced with permission from [19].

G-Ins: G-insulin; MSN: Mesoporous silica nanoparticle.

Polymer



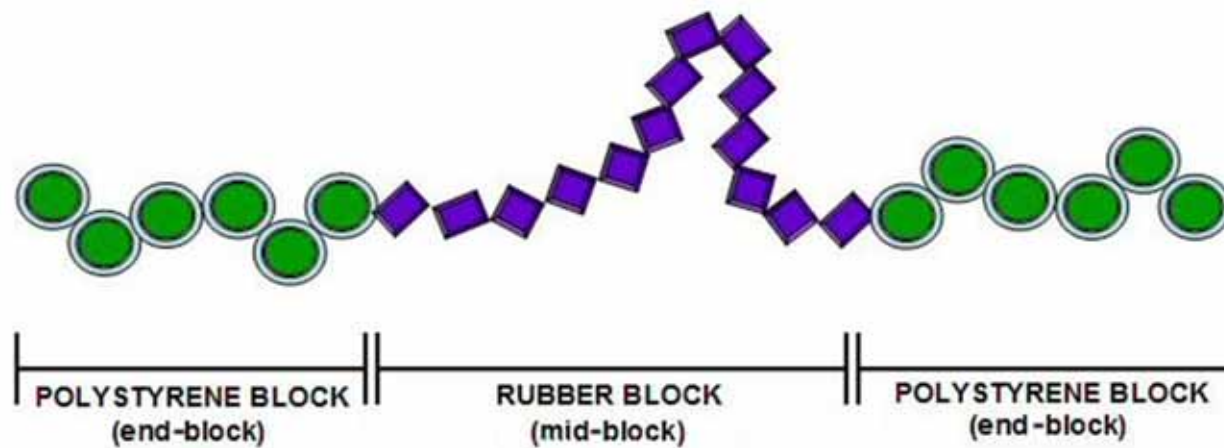
a monomer ethene



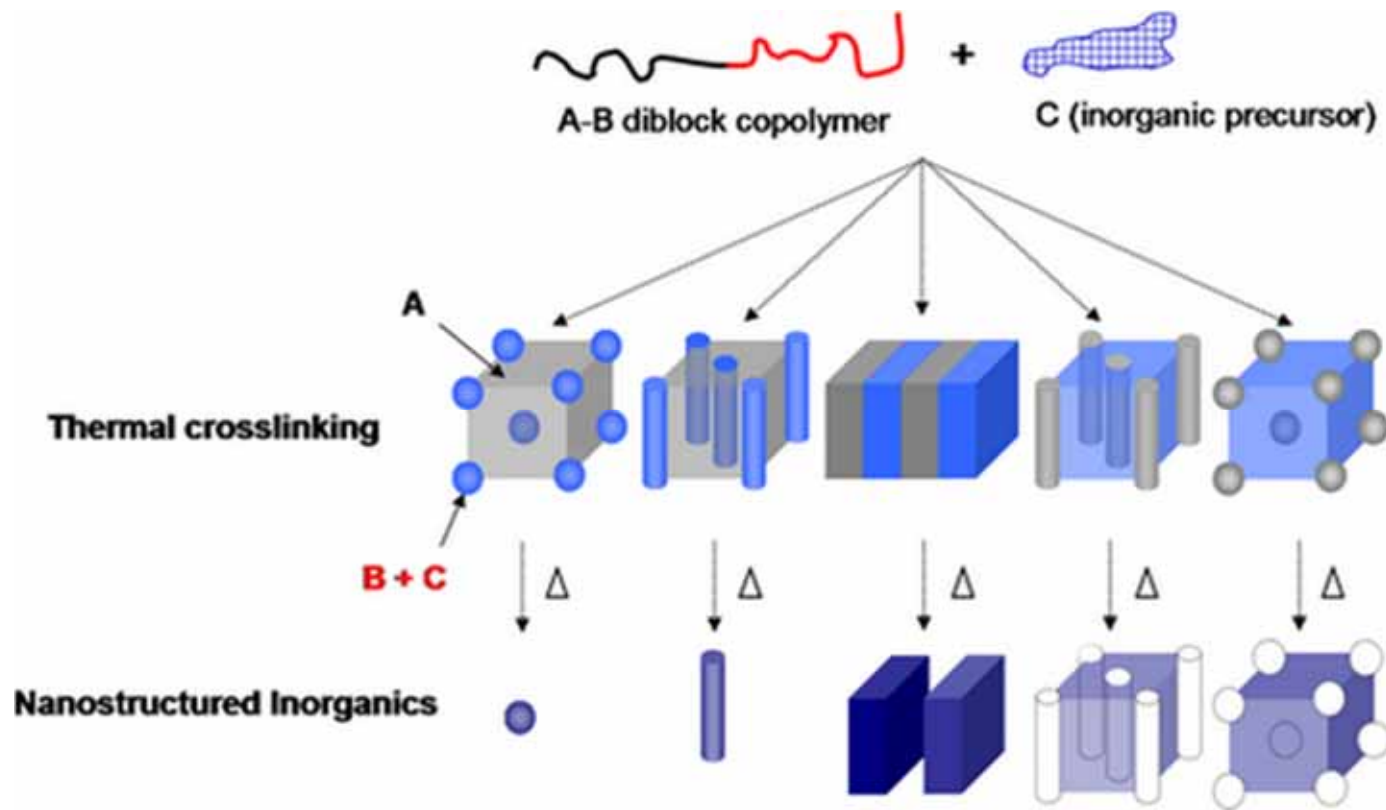
a polymer

poly(ethene)

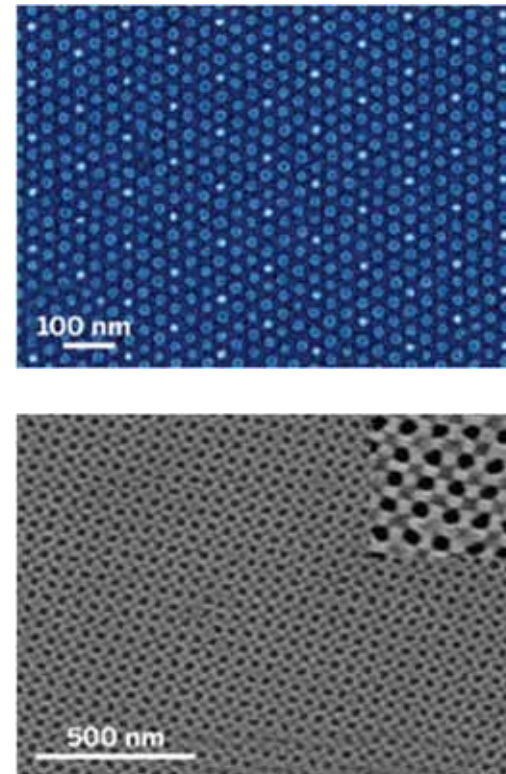
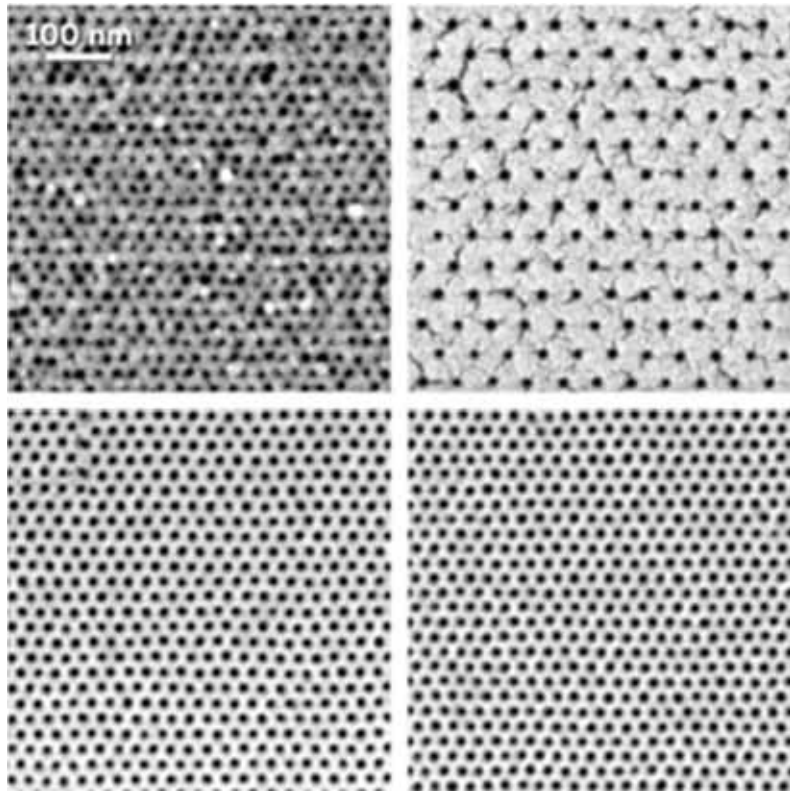
Block copolymer



Phase Segregation



Self-Assembled Block-copolymer



CNT

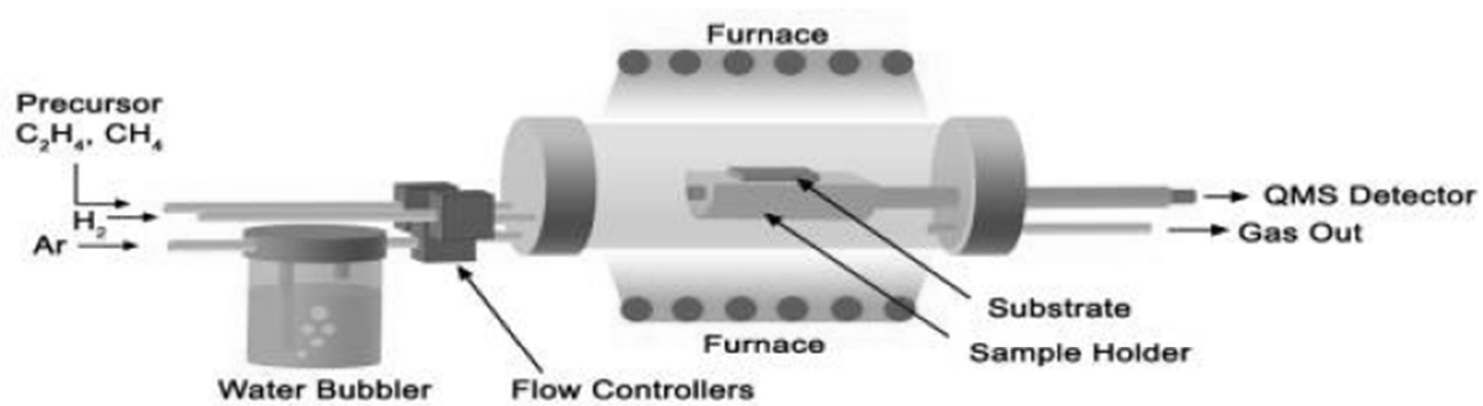
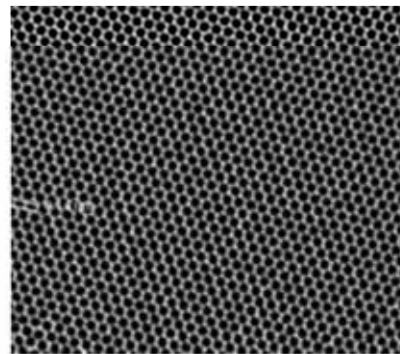
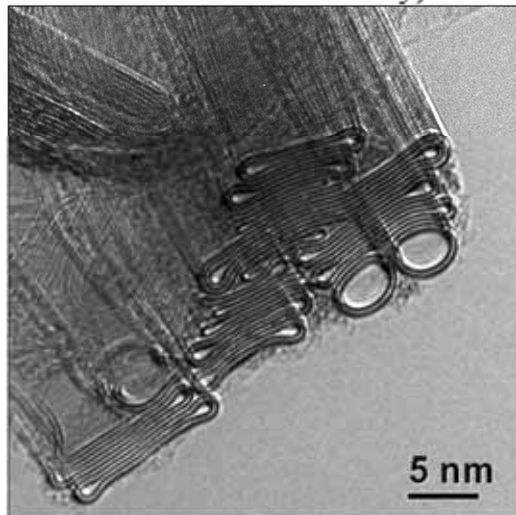


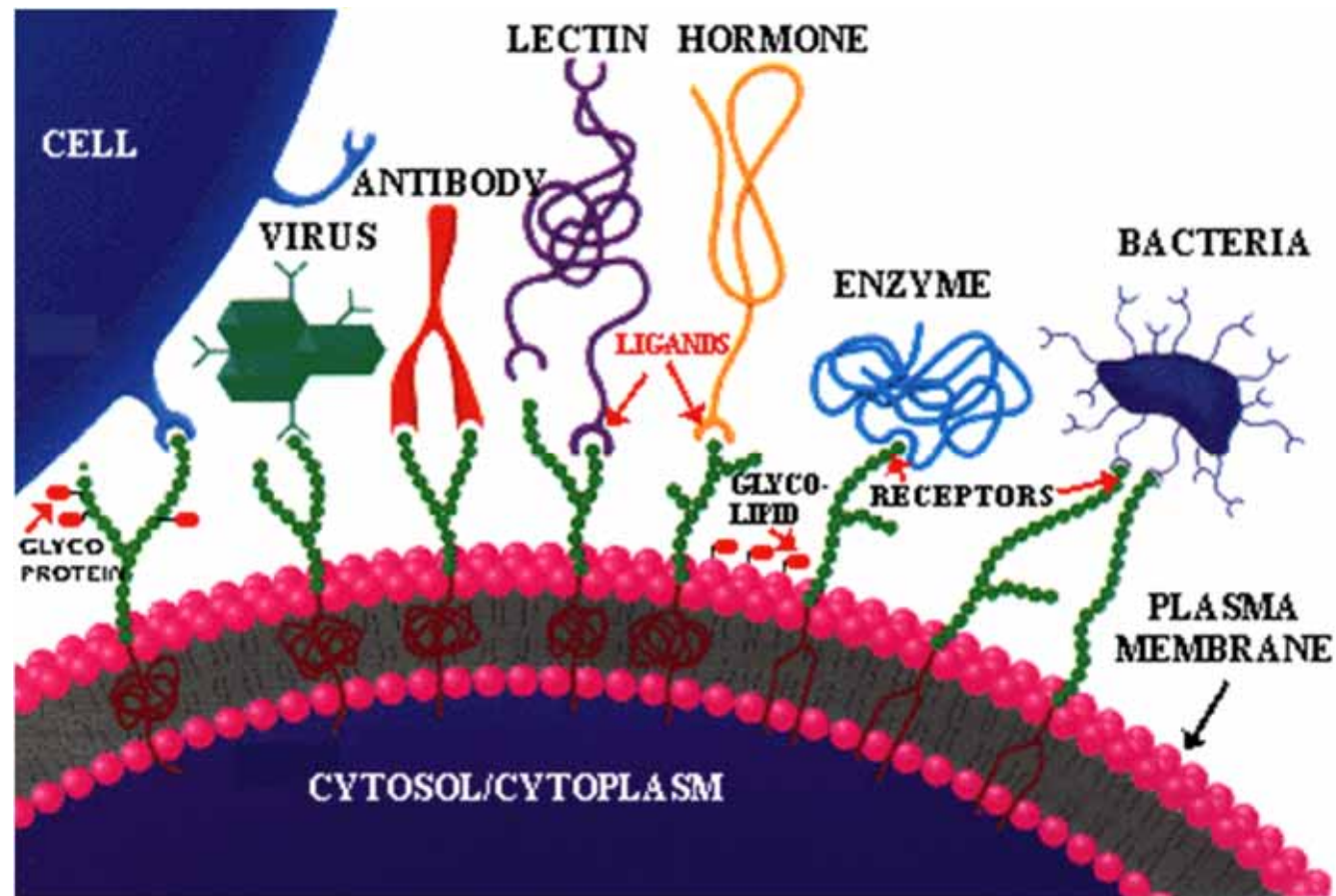
Fig. 1. Schematic of a CVD reactor for carbon nanotube growth. (Sketch by S. Yarmolenko from NCA&T State University)



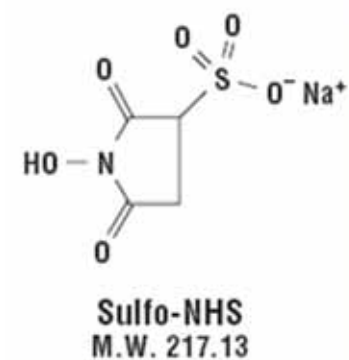
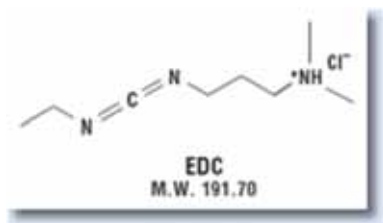
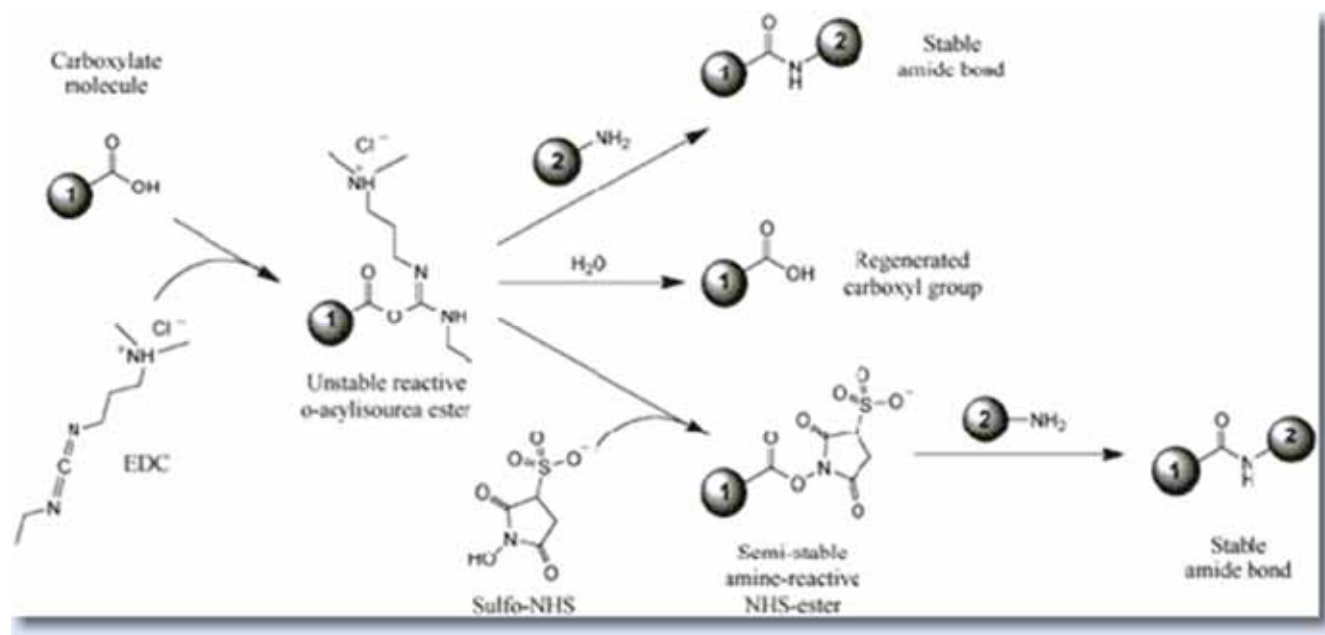
Surface Functionalization

- Recognition
 - Molecular Recognition
 - Protein
 - DNA
 - Saccharide
- Reporting/Detection
 - Dye
 - Quantum dots
 - SPR
 - SERS/LSPR
- Separation
 - Gel/Chromatography
 - Magnetic
- Surfaces
 - Gold and silver
 - Silicon oxide (glass)
 - Quantum dots
 - Polymer

Molecular Recognition

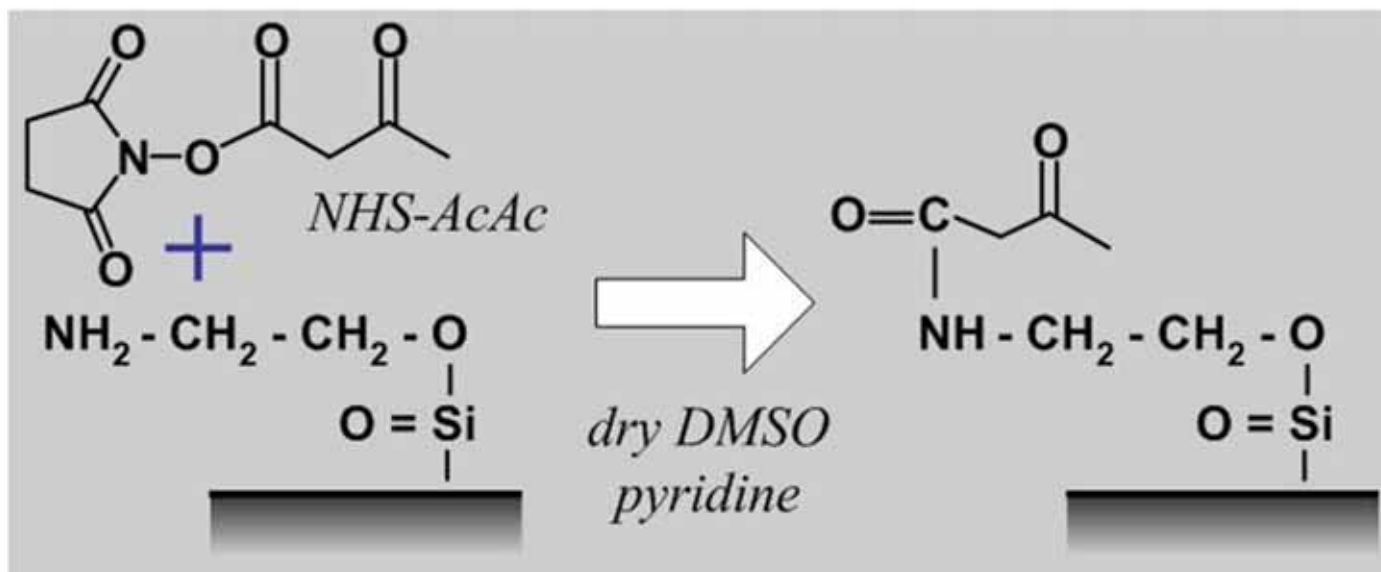


Carboxyl Presenting Surfaces

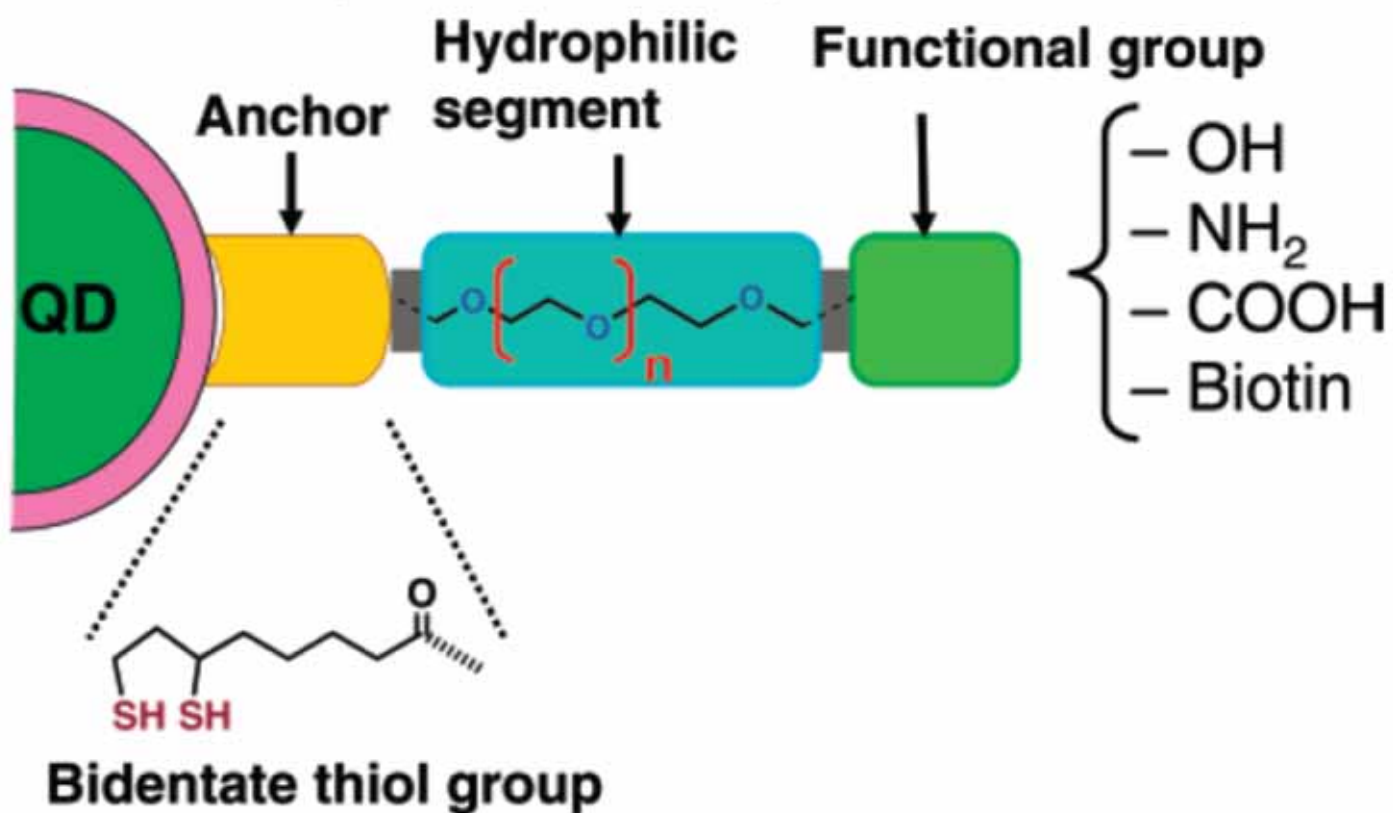


EDC (1-Ethyl-3-[3-dimethylaminopropyl]carbodiimide Hydrochloride)

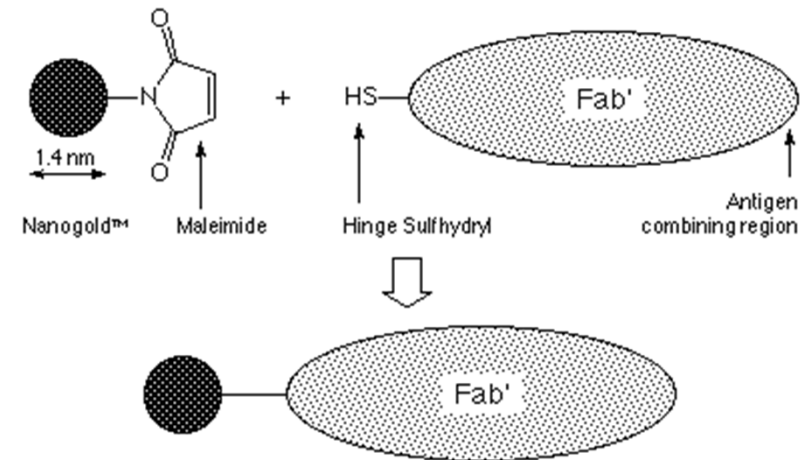
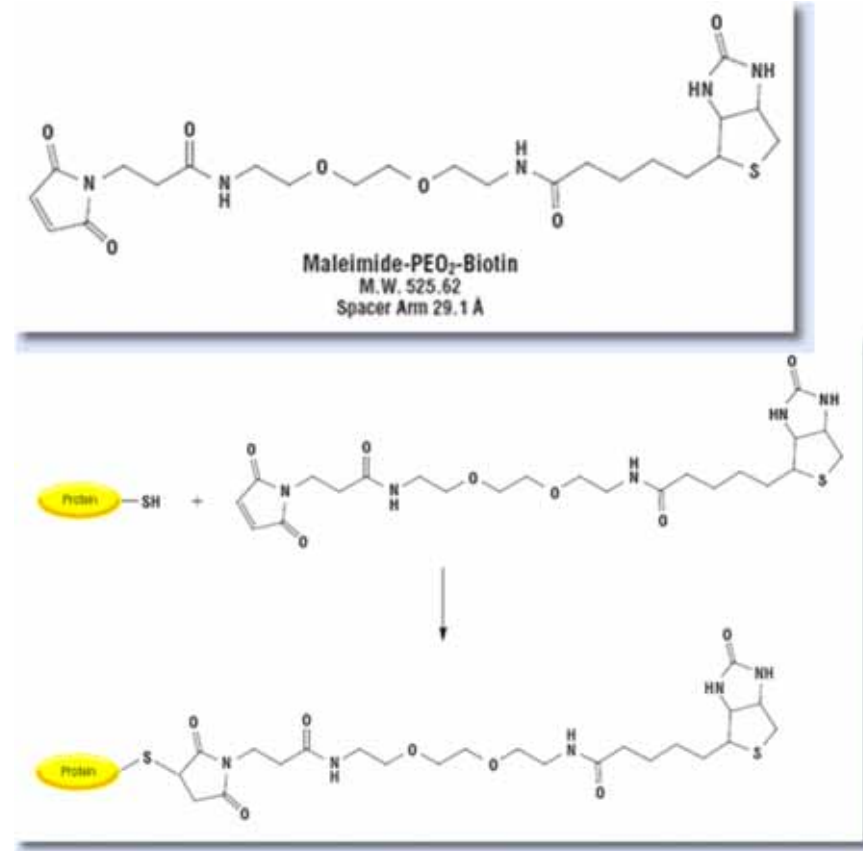
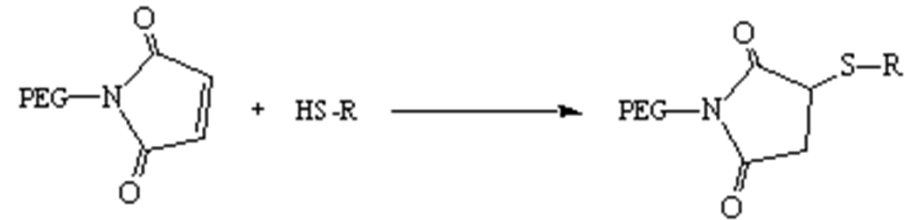
Amine Presenting Surface



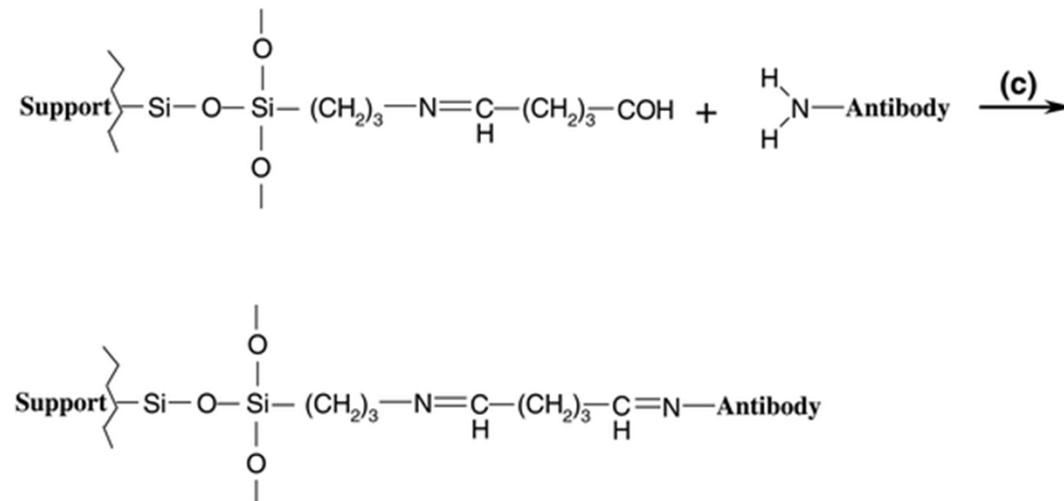
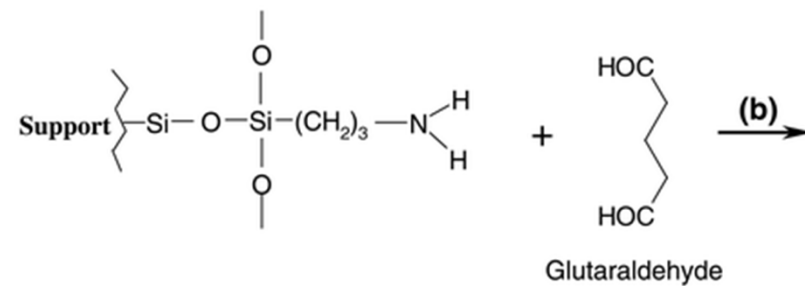
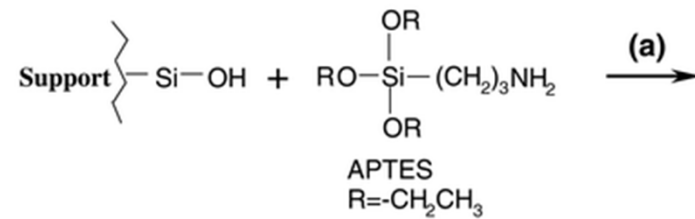
Scheme 1. Modular Design of Hydrophilic Ligands with Terminal Functional Groups Used in This Study



Sulfhydryl Labeling



Silica Modification



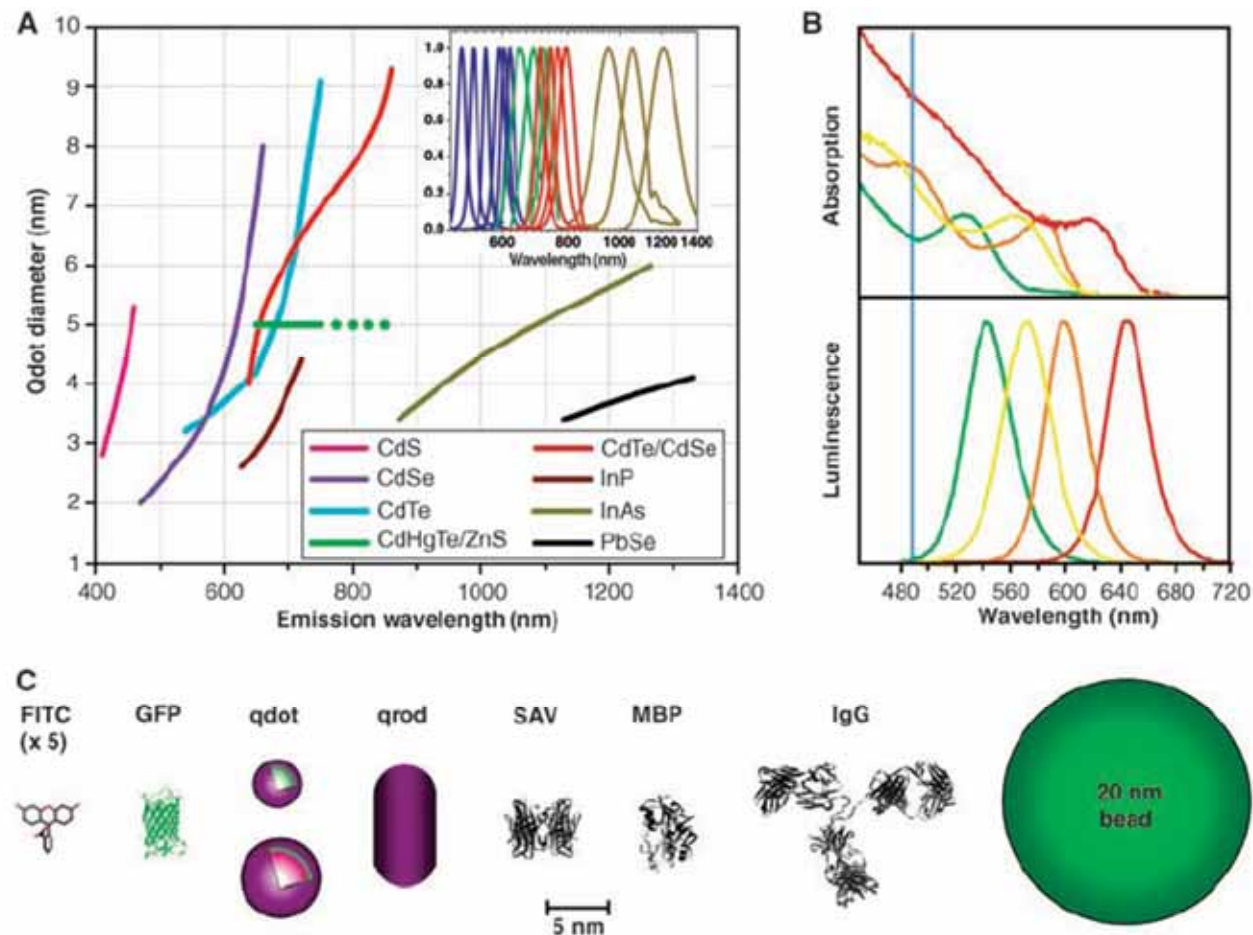
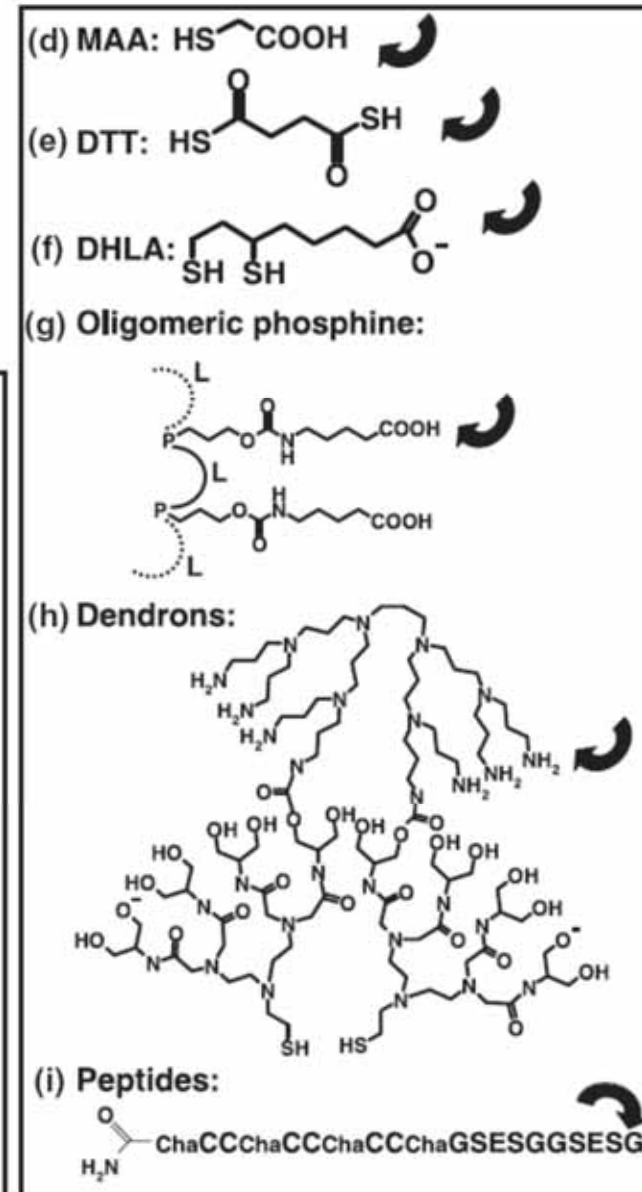
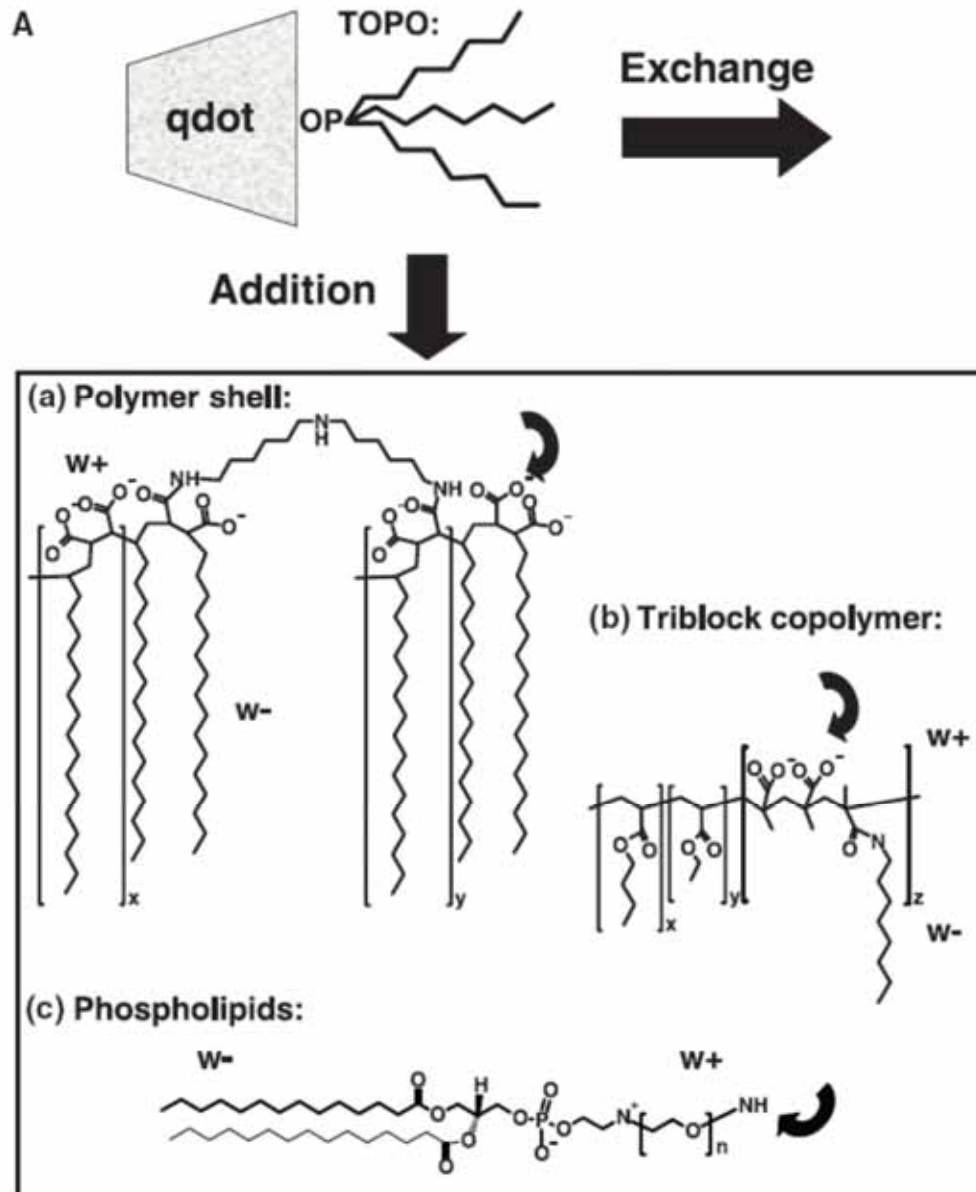
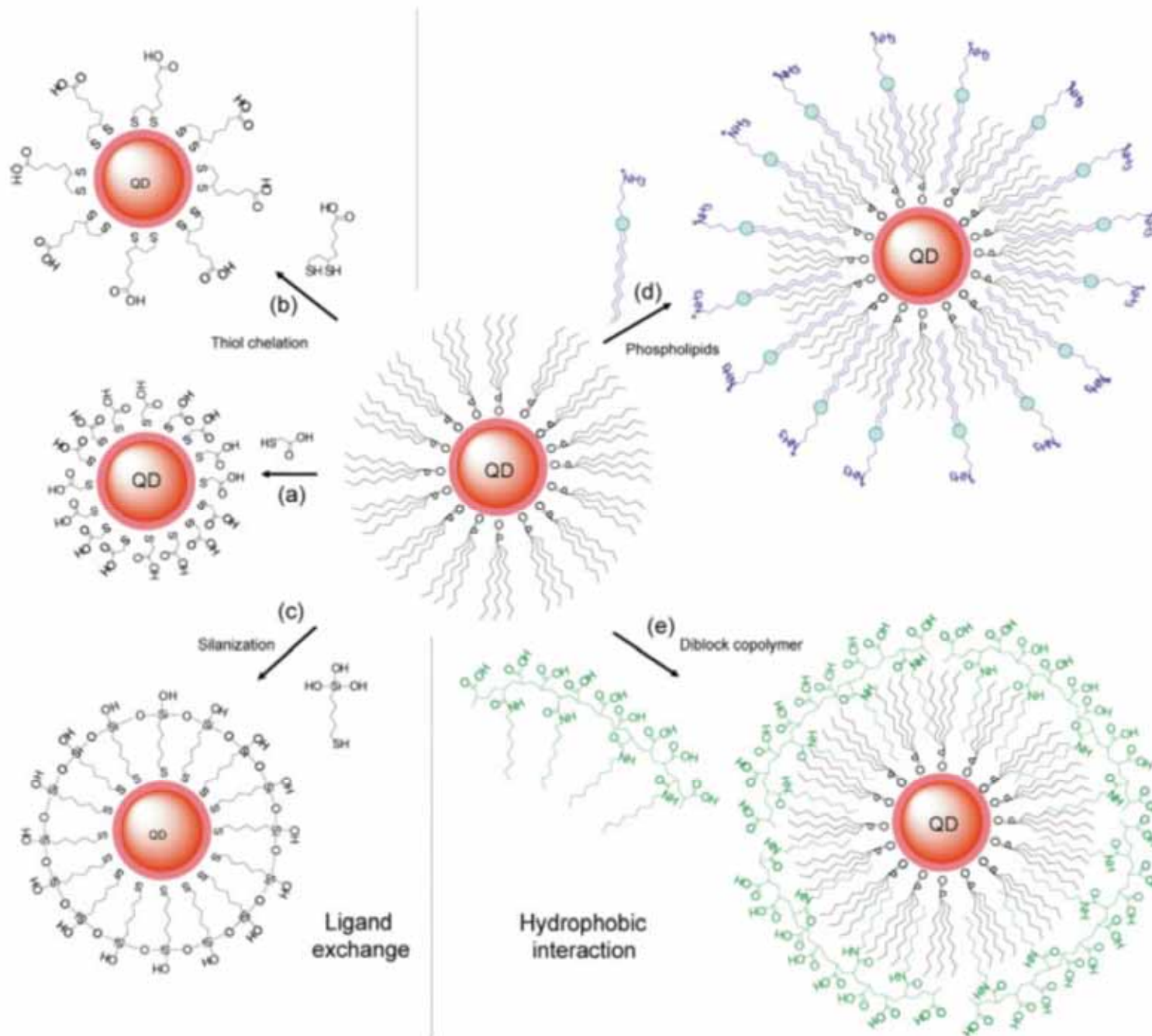


Fig. 1. (A) Emission maxima and sizes of quantum dots of different composition. Quantum dots can be synthesized from various types of semiconductor materials (II-VI: CdS, CdSe, CdTe...; III-V: InP, InAs...; IV-VI: PbSe...) characterized by different bulk band gap energies. The curves represent experimental data from the literature on the dependence of peak emission wavelength on qdot diameter. The range of emission wavelength is 400 to 1350 nm, with size varying from 2 to 9.5 nm (organic passivation/solubilization layer not included). All spectra are typically around 30 to 50 nm (full width at half maximum). Inset: Representative emission spectra for some materials. Data are from (12, 18, 27, 76–82). Data for CdHgTe/ZnS have been extrapolated to the maximum emission wavelength obtained in our group. (B) Absorption (upper curves) and emission (lower curves) spectra of four CdSe/ZnS qdot samples. The blue vertical line indicates the 488-nm line of an argon-ion laser, which can be used to efficiently excite all four types of qdots simultaneously. [Adapted from (28)] (C) Size comparison of qdots and comparable objects. FITC, fluorescein isothiocyanate; GFP, green fluorescent protein; qdot, green (4 nm, top) and red (6.5 nm, bottom) CdSe/ZnS qdot; qrod, rod-shaped qdot (size from Quantum Dot Corp.'s Web site). Three proteins—streptavidin (SAV), maltose binding protein (MBP), and immunoglobulin G (IgG)—have been used for further functionalization of qdots (see text) and add to the final size of the qdot, in conjunction with the solubilization chemistry (Fig. 2).





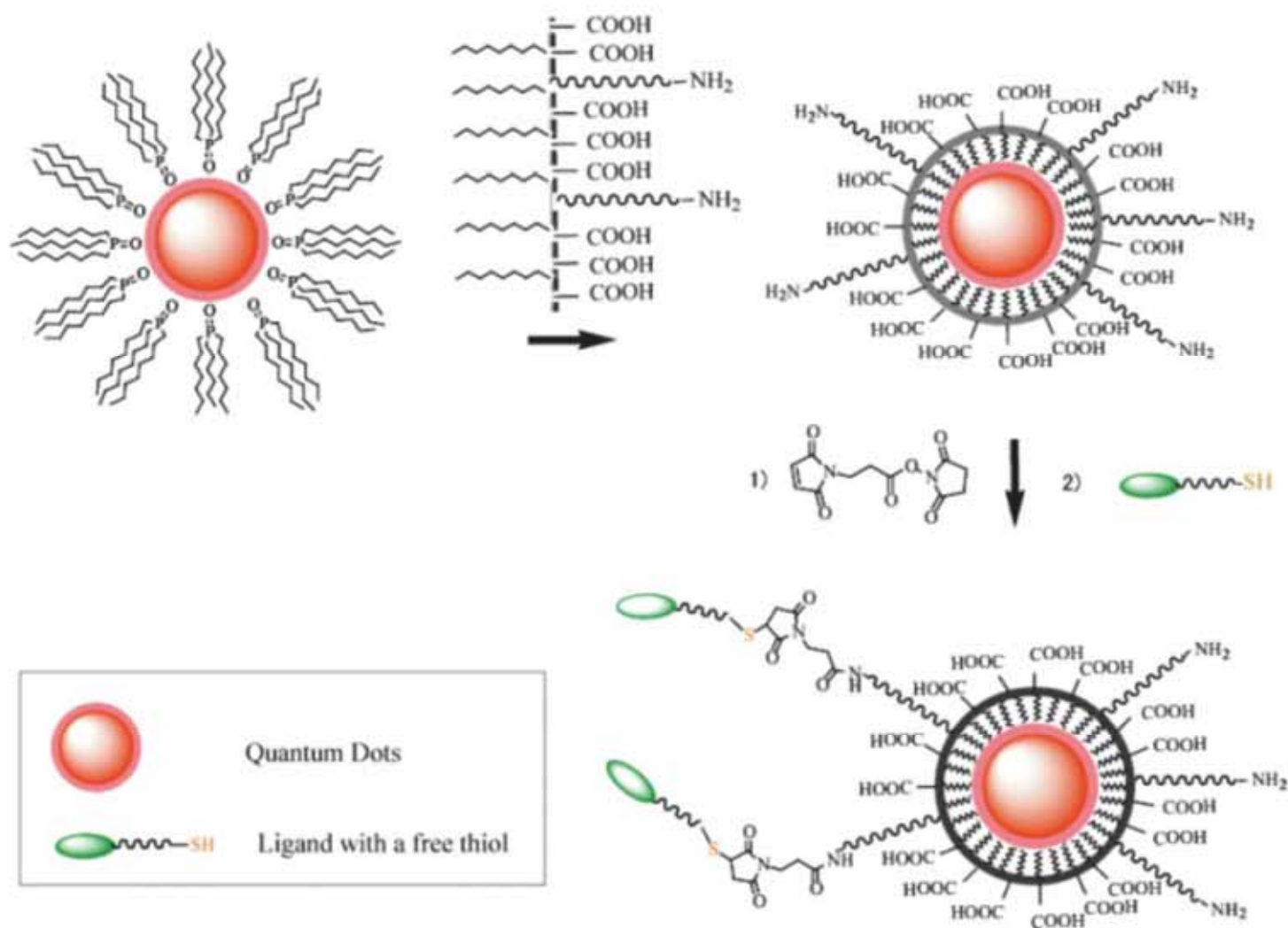


FIGURE 3 Maleimide functionalized QDs for conjugating thiol-containing ligands. TOPO stabilized QDs are coated with a primary amine functionalized tri-block amphiphilic copolymer for producing water-soluble QDs, which facilitate further conjugation to ligands with free thiols through bi-functional cross-linkers.